JCI The Journal of Clinical Investigation

Myeloid cell-derived PROS1 inhibits tumor metastasis by regulating inflammatory and immune responses via IL-10

Avi Maimon, Victor Levi-Yahid, Kerem Ben-Meir, Amit Halpern, Ziv Talmi, Shivam Priya, Gabriel Mizraji, Shani Mistriel-Zerbib, Michael Berger, Michal Baniyash, Sonja Loges, Tal Burstyn-Cohen

J Clin Invest. 2021. https://doi.org/10.1172/JCI126089.

Research In-Press Preview Inflammation Oncology

Graphical abstract

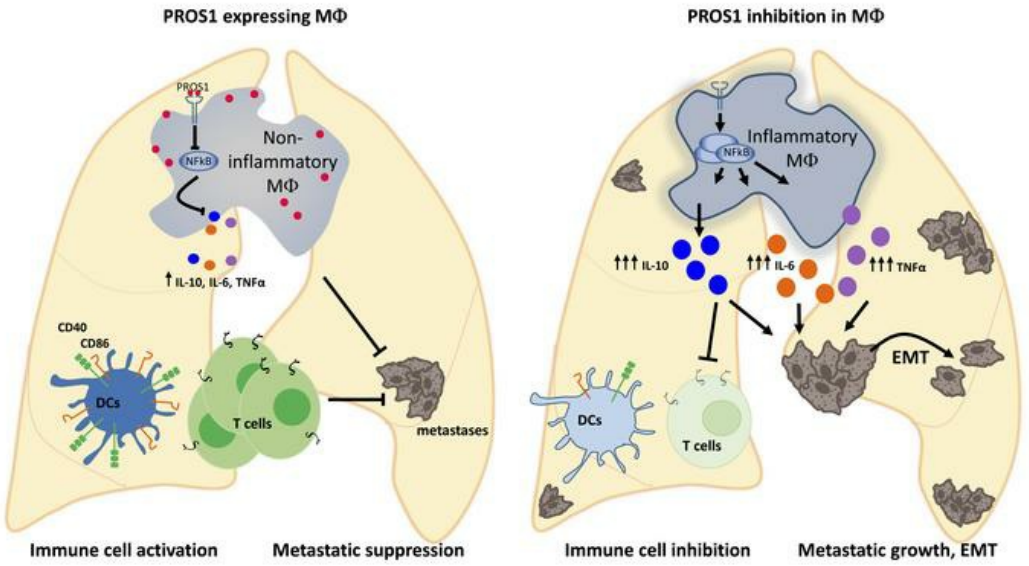

Find the latest version:

https://jci.me/126089/pdf

Myeloid cell-derived PROS1 inhibits tumor metastasis by regulating inflammatory and immune responses via IL-10

Avi Maimon[1], Victor Levy-Yahid[1], Kerem Ben-Meir[2] Amit Halpern[1], Ziv Talmi[1], Shivam Priya[1], Gabriel Mizraji[1], Shani Mistriel-Zerbib[2], Michael Berger[2], Michal Baniyash[2], Sonja Loges[3,4] and Tal Burstyn-Cohen[1*]

[1]The Institute for Dental Sciences, Faculty of Dental Medicine, The Hebrew University, Jerusalem, Israel.

[2]The Lautenberg Center for Immunology and Cancer Research, Israel-Canada Medical Research Institute, Faculty of Medicine, The Hebrew University, Jerusalem, Israel.

[3]Division of Personalized Medical Oncology (A420), German Cancer Research Center (DKFZ), Heidelberg, Germany.

[4]Department of Personalized Oncology, University Hospital Mannheim, Mannheim, Germany

Keywords:

Protein S, PROS1, Inflammation, Tumor-microenvironment interactions, TME, IL-10

***Corresponding Author:**
Tal Burstyn-Cohen
The Institute for Dental Sciences, Faculty of Dental Medicine, The Hebrew University, Jerusalem, 9112001, Israel.
Tel: +972-2-6758582
talbu@mail.huji.ac.il

Conflict of interest statement

The authors have declared that no conflict of interest exists.

Abstract

Stimulation of TAM (TYRO3, AXL and MERTK) Receptor Tyrosine Kinases promotes tumor progression through numerous cellular mechanisms. TAM cognate ligands GAS6 and PROS1 (for TYRO3 and MERTK) are secreted by host immune cells, an interaction which may support tumor progression. Here we reveal an unexpected anti-metastatic role for myeloid-derived PROS1, directly suppressing the metastatic potential of lung and breast tumor models. *Pros1* deletion in myeloid cells led to increased lung metastasis, independent of primary tumor infiltration. PROS1-cKO BMDMs led to elevated TNFα, IL-6, Nos2 and IL-10 via modulation of the *Socs3*-NFκB pathway. Conditioned medium from cKO BMDMs enhanced EMT, ERK, AKT and STAT3 activation within tumor cells, and promoted IL-10 dependent invasion and survival. Macrophages isolated from metastatic lungs modulated T cell proliferation and function, as well as expression of costimulatory molecules on dendritic cells in a PROS1-dependent manner. Inhibition of MERTK kinase activity blocked PROS1-mediated suppression of TNFα and IL-6, but not of IL-10. Overall, using lung and breast cancer models, we identify the PROS1-MERTK axis within BMDMs as a potent regulator of adaptive immune responses with a potential to suppress metastatic seeding, and reveal IL-10 regulation by PROS1 to deviate from that of TNFα and IL-6.

Introduction

Macrophages play dominant roles in tumor-microenvironment (TME) interactions affecting tumor growth and metastasis. By secreting various factors, macrophages can alter tumor cell behavior, often promoting cancer initiation and supporting metastatic progression (1–4). The bi-directional cross-talk between tumor cells and macrophages was shown to modulate tumor growth and metastasis through several mechanisms (5). Examples include macrophage polarization towards an M2-like immunosuppressive phenotype by tumor-secreted lactic acid (6) and the induction of the proinflammatory cytokines tumor necrosis factor-α (TNFα) and interleukin-6 (IL-6) within macrophages by tumor-derived Versican, leading to increased metastasis (7). Another macrophage-mediated tumor-promoting pathway includes the secretion of molecules which activate proto-oncogenes expressed by tumor cells. This was shown for Growth-arrest-specific 6 (Gas6) which is upregulated by tumor-infiltrating macrophages. GAS6 leads to increased tumor growth and metastasis, by stimulating its cognate receptors TYRO3, AXL and MERTK, constituting the TAM family of receptor tyrosine kinases (RTKs) (8) also identified as proto-oncogenes (9). We therefore reasoned that Protein S (PROS1), a TAM agonist with high homology to GAS6, also expressed by immune cells would likewise activate TAM receptor (TAM-R) oncogenic signaling through tumor-immune cell interactions. Because TME interactions modulate tumor growth and metastasis, identifying the factors underlying these interactions is of great importance.

As a ligand for the proto-oncogenic TAM-Rs, we recently reported the upregulation of PROS1 in oral squamous cell carcinoma (OSCC), where PROS1 supported OSCC aggressiveness though AXL activation. Inhibition of PROS1 repressed tumor cell phenotypes both in-vitro and in-vivo (10), indicating its tumor-promoting capacity. In addition to their oncogenic capabilities, TAMs are key regulators of immune response and inflammation (11–14). Activation of TAM-Rs in immune cells by their agonists GAS6 and PROS1 alleviates the immune response and mitigates inflammation (14–

16). Respectively, TAM inhibition is pro-inflammatory, as seen in mice following genetic inactivation of TAM-Rs (17–20) and ligands (15, 16). Using a zymosan-induced model of peritonitis, we recently identified PROS1 as a regulator of peritoneal macrophage polarization also mediating their phagocytic clearance of apoptotic neutrophils - both essential elements contributing to the resolution of inflammation (16).

In this study, we investigate the role of PROS1 in the myeloid compartment of the TME. We find that myeloid-derived PROS1 inhibits tumor metastasis through tempering peripheral inflammation and immune modulation rather than by directly stimulating TAM-dependent oncogenic signaling within tumor cells. Conditional knockout (cKO) of *Pros1* in myeloid cells results in their hyper-inflammatory profile and increased infiltration into metastatic lungs, as well as elevated levels of the extracellular degrading enzyme matrix metalloprotease 9 (MMP9). Direct effects on tumor cells led to epithelial-to-mesenchymal transition (EMT) and improved survival and invasiveness. Concomitantly, inhibition of PROS1 expression affected both dendritic cell (DC) maturation and T cell proliferation and activation. Together, our findings reveal PROS1 as a key player acting at multiple levels on both the tumor cells and the TME, directly impacting metastasis. Moreover, our data indicate that PROS1 expression in myeloid cells dictates the inflammatory status of the lungs. We further show that PROS1 is a key molecular switch of inflammatory signaling within bone marrow-derived macrophages (BMDMs), modulating the NFκB pathway. Addition of PROS1 to *Pros1*-cKO BMDMs suppresses their pro-inflammatory signature, and reverts their pro-metastatic capacity in-vivo. Mechanistically, we reveal that inhibiting the MERTK kinase activity blocked PROS1-mediated suppression of TNFα and IL-6, but did not affect that of IL-10. Investigating the relevance of the PROS1/IL-10 axis revealed that IL-10 acts directly on tumor cells to increase their survival and invasive potential, while inhibiting T cell proliferation at the same time, which is suppressed upon addition of PROS1 or by IL-10 neutralization. Taken together, our data identify PROS1 as a novel anti-metastatic protein, acting at multiple levels. PROS1 (i) directly

affects EMT and cancer cell survival, (ii) modulates DC and T cell function and (iii) regulates inflammatory signaling in metastasis-associated macrophages, directly impacting the metastatic potential.

Results

***Pros1* deficiency in host myeloid cells exacerbates tumor metastasis.**

To test whether PROS1 in host myeloid cells affects cancer progression we genetically deleted *Pros1* expression in the myeloid lineage by crossing *Pros1*$^{fl/fl}$ mice (21) to *LysM-Cre*$^{+}$ mice (22), efficiently driving Cre expression in myeloid cells. *Pros1*$^{fl/fl}$ (control) and *LysM*-Cre^{+}*;Pros1*$^{fl/fl}$ conditional knockout mice (hereafter *Pros1*-cKO) were challenged with a subcutaneous injection of murine Lewis Lung Carcinoma (LLC) cells (23). Primary tumor growth dynamics in control and *Pros1*-cKO mice were comparable for the duration of the experiment (fig 1A and fig S1A). However, metastatic burden was significantly increased in the lungs of *Pros1*-cKO mice compared with their littermate controls (fig 1B-E). Histopathological analysis of lung sections revealed larger lung metastases in *Pros1*-cKO mice (0.2 ± 0.02 mm^2) compared to controls (0.09 ± 0.04 mm^2; fig 1C-E). *Pros1*-cKO lungs also showed increased numbers of metastatic foci (4 ± 1.2) compared to controls (1.1 ± 0.5; fig 1E). We also tested the effect of Myeloid *Pros1* expression on tumor growth and metastasis using the AT3 mammary carcinoma model (fig 1F-J). Akin to the lung cancer model, primary tumor growth of orthotopically-injected GFP-expressing AT3 cells was similar between control and *Pros1*-cKO mice (fig 1F and fig S1B-C). Although no significant differences in the number of metastatic foci (fig 1J), metastasis in *Pros1*-cKO mice were larger (0.198 ± 0.05 mm^2) than in controls (0.06 ± 0.03 mm^2; fig 1I). These results indicate that ablation of *Pros1* in host myeloid cells minimally affects primary tumor growth, but significantly enhances metastasis of syngeneic models of mammary and

lung cancers, indicating an inverse association between metastasis and host myeloid PROS1 expression. This association reveals an unanticipated, yet decisive anti-metastatic role for host immune cell-derived PROS1.

Pros1 ablation in myeloid cells induces lung inflammation increasing their permissiveness for tumor cell colonization.

As a ligand for the TAM-Rs, PROS1 takes a cell autonomous negative regulatory function in the immune response of DCs and in the regulation of DCs by T cells (12–15). Inactivation of TAM-R signaling in mice results in a chronically activated immune system, autoimmune disease, and a pro-inflammatory cytokine signature (12, 20). These phenotypes notwithstanding, the inflammatory status of mice lacking PROS1 in the myeloid lineage, and its possible impact on cancer have not been investigated. We hypothesized that lack of PROS1 in the myeloid compartment may cause systemic or local inflammation in the lungs, previously demonstrated to promote metastasis in several cancer models (24–26). Indeed, lungs of *Pros1*-cKO mice expressed higher baseline levels of tumor necrosis factor alpha (*Tnf*α) and nitric oxide synthase 2 (*Nos2),* without changes in the *p35* subunit of *Il-12*, along with decreased expression of the suppressor of cytokine signaling 3 (*Socs3*) (fig 2A). Interestingly, mRNA levels of the anti-inflammatory cytokine *Il-10* were concomitantly elevated (fig 2A). TNFα, IL-6 and IL-10 protein levels were also higher in cKO lungs, which became more pronounced after tumor challenge (fig 2B). This pro-inflammatory signature was restricted to the lungs, as TNFα and IL-6 protein in the plasma remained at basal levels and were similar between control and *Pros1*-cKO mice (fig 2C).

Analysis of immune cell infiltration revealed elevated ratios of total myeloid cells ($CD11b^{+}$) and monocytes ($Ly6C^{hi}Ly6G^{-}$) in *Pros1*-cKO lungs, with a non-significant increase in granulocytes ($Ly6G^{+}Ly6C^{lo}$) (fig. 2D-E). Pulmonary macrophages are heterogeneous, with alveolar macrophages (AM) residing in the airway lumen highly

expressing the integrin CD11c but not CD11b, and interstitial macrophages (IM) located within the lung interstitial space together with dendritic cells (DCs), another myeloid population expressing PROS1. IMs are distinguished from AMs due to their high CD11b/F4/80 and low CD11c expression (27, 28). Whereas AM and DC populations were comparable between control and cKO mice, IM frequencies were significantly elevated in lungs of cKO mice (fig. 2F, G). Originating from circulating monocytes (29), IMs regulate lung immune homeostasis, and provide immune-suppressive functions through elevated secretion of IL-10 (28). By contrast to the metastatic site, no differences were observed in monocytes ($Ly6C^+Ly6G^-$), granulocytes ($Ly6G^+Ly6C^+$) or macrophage ($F4/80^+$) frequencies in the primary tumor (fig. S2A-B). Taken together, these results indicate that loss of PROS1 in the myeloid compartment is sufficient to induce lung inflammation.

We next tested whether inflammation in *Pros1*-cKO lungs provides a permissive environment for metastatic cells by assessing in-vivo survival and colonization following intravenous injecting of LLC-GFP^+ cells. Dissemination and colony formation in *Pros1*-cKO lungs was enhanced 21 days later, with more superficial GFP-expressing metastatic foci (fig S2C). Scoring LLC-GFP^+ cells by FACS revealed *Pros1*-cKO lungs had 3.6-fold more GFP^+ cells compared to controls (fig S2D). Lungs from these *Pros1*-cKO mice also expressed higher *Tnfa*, *Nos2* and *Il-12*p35 levels (fig S2E), correlative with increased colonization of the lungs. We found that inflammation in *Pros1*-cKO lungs preceded metastatic seeding: elevated *Tnfα, Il-6* and *Nos2* production was recorded as early as 10 days post inoculation, prior to any visually-detected metastases, and remained elevated, with the addition of *Il-10* at 20 days post inoculation (fig S2F-G). Thus, our results indicate that inflamed lungs of *Pros1*-cKO mice support enhanced colonization and metastasis formation by LLC cells. Similar results following intravenous injection implies metastasis is independent of any interactions at the primary tumor site.

Expression of *Pros1* in lung-infiltrating bone marrow derived myeloid cells determines lung inflammation.

We hypothesized the elevated frequencies of *Pros1*-deficient myeloid cells provoking a pro-tumor effect originate from the circulation, as seen in a variety of cancer models (1, 3, 11, 30). Particularly in LLC, infiltrating macrophages exacerbate lung metastasis (31) whereas macrophage deficiency attenuates LLC tumor growth and metastasis in *op/op* mice lacking CSF-1 (32). Monocytes and tumor-associated macrophages also facilitate metastasis in a PyMT mammary tumor model (33–35). Bone marrow (BM)-derived inflammatory monocytes, IMs and AMs all support a pre-metastatic niche (33, 36, 37). To understand whether metastatic lungs display the same immune infiltrating profile as tumor-naïve mice, F4/80^{+} cells were sorted from tumor-harboring mice, and characterized both immunologically and for their cytokine expression. Similar to naive cKO lungs which had elevated IMs (fig 2F-G), F4/80^{+} cells from cKO metastatic lungs expressed CD11b^{hi} but very low CD11c, resembling the IM profile (fig 3A-B). Within F4/80^{+} sorted cells from metastatic cKO mice, the fraction of Ly6C^{hi} increased, along with a decrease in Ly6C^{lo} cells (fig 3B), indicating a trend towards monocyte (Ly6C^{hi}) enrichment with a higher pro-inflammatory profile (38). The expression of *Tnfa, Il-6, Nos2* and *Il-10* in F4/80^{+} macrophages sorted from cKO, but not control lungs confirmed their inflammatory nature in an in-vivo metastatic setting (fig 3C).

We next sought to test whether BM-derived cells can modify lung inflammation in a *Pros1*-dependent manner. For this, the BM of lethally irradiated control and *Pros1*-cKO mice was reconstituted with BM from the reciprocal genotype. *Pros1*-exprssing BM control (*LysM*-Cre^{+}; *Pros1*$^{+/+}$;Ai9$^{TdT\text{-}LSL}$) carried the tomato red reporter (Ai9$^{TdT\text{-}LSL}$) for monitoring reconstitution efficiency. Under such conditions, the recipient-BM population is lethally irradiated, while the radio-resistant AMs are relatively unaffected (39). Eight weeks later, we verified efficient reconstitution by TdT expression in the circulation of recipient mice. Analyzing the blood of recipient cKO mice reconstituted with TdT-labelled PROS1-expressing BM (*Pros1*$^{+/+}$*;LysM-Cre*$^{+;TdT}$→cKO) revealed TdT signal,

resembling the endogenous TdT levels in naive mice (fig S3A-D). Moreover, the lungs of transplanted cKO mice were infiltrated by TdT expressing donor myeloid cells, (fig 3D). Assessing the inflammatory status of cKO→*Pros1*$^{fl/fl}$ lungs revealed elevated *Tnf*a and *Nos2* transcripts with low *Il-10* levels (fig 3E, blue bars). By contrast, lungs of cKO mice reconstituted with TdT-labeled *Pros1*$^{+/+}$ BM (*Pros1*$^{+/+}$*;LysM-Cre*$^{+}$*;*^{TdT}→cKO) had low levels of pro-inflammatory cytokines and higher *Il-10* levels (fig 3E, green bars), even though they had expressed high *Tnfa* and *Nos2* levels prior to BM transfer (fig 2A). The spleens of transplanted mice were also successfully populated with donor cells with similar induction of *Tnfa*, although *Nos2* levels remained unaffected (fig S3E), indicating a differential effect for BM-derived PROS1 on spleen and lung tissue. Thus, PROS1-expressing myeloid cells transplanted into inflamed cKO hosts (fig 3D-E) reversed their pro-inflammatory profile, and *Pros1*-deficient BM was reciprocally sufficient to elevate lung inflammation in otherwise non-inflamed control mice. To determine whether the inflammatory status of the lungs directly contributes to the metastatic burden, we challenged reciprocally transplanted mice with LLC-Luc^{+} cells and assessed metastasis. Successful reconstitution in tumor-bearing mice was verified by TdT expression (fig S3F). At endpoint, cKO mice transplanted with control BM had less metastasis, while the reciprocally transplanted mice (controls receiving cKO BM) had elevated occurrences of metastasis, seen superficially and evidenced by luciferin expression (fig 3F-G). As for tumor naïve transplanted mice, cytokine expression in tumor-bearing control mice transplanted with cKO BM was elevated. However, compared to tumor-naïve mice, the magnitude of inflammation was elevated, pointing to the contribution of metastatic cells to the overall inflammatory profile (fig 3H). Specifically, *Il-10* levels significantly increased in tumor-bearing control mice which received cKO BM, suggesting a positive role for LLC cells in IL-10 expression within the tumor microenvironment.

Taken together, we identified IMs as a myeloid-specific BM-derived population affecting lung inflammation in a PROS1-dependent manner, and show that the inflammatory status of the lungs is a major factor contributing to lung metastasis.

PROS1 reduces inflammatory cytokine production in BMDMs through regulation of the NFκB pathway.

The observation that PROS1-deficient BM-derived F4/80^{+} infiltrating cells are proinflammatory prompted us to investigate the mechanism by which PROS1 regulates inflammation in these cells. For this, we generated BMDMs from control (BMDM$^{fl/fl}$) and *Pros1*-cKO (BMDM^{cKO}) mice (fig S4). BMDM^{cKO} exhibited higher transcript levels of *Tnfa*, *Nos2, Il-6*, *Il-10* and lower *Socs3* mRNA (fig 4A). TNFα, IL-6 and IL-10 cytokine secretion was also higher in BMDM^{cKO} (fig 4B). Given the possible compensatory and redundant functions of GAS6 and MERTK in macrophages (20, 40–42), we measured expression of both genes in BMDM^{cKO}, which were unchanged (fig 4C).

To dissect the molecular pathway underlying PROS1-mediated regulation of inflammation, we monitored the activation status of NFκB, a key regulator of cytokine production and previously shown to function downstream of TAM signaling (41), including in monocytes (17). Inhibition of NFκB activation by GAS6 was shown in bone-marrow-derived dendritic cells (BM-DCs) (14) and in splenic-derived DCs by PROS1 secreted from T cells (15). However, the effect of PROS1 on NFκB in macrophages is unknown. Under baseline conditions, pNFκB levels were significantly elevated in BMDM^{cKO} (fig 4D-E), consistent with elevated TNFa, IL-6 and decreased *Socs3* levels recorded in these cells (fig 4A-B).

To assess the dynamics of NFκB phosphorylation, serum-starved BMDMs were stimulated with LPS. Contrary to control cells, where NFκB activation was transient, in BMDM^{cKO}, high levels of pNFκB persisted 1 hr after stimulation (fig 4F-G). Additionally, levels of the NF-κB inhibitor IκBα were significantly lower in BMDM^{cKO} (Fig 4H-I).

Notably, the basal levels of IκBα at steady state (time point 0) were significantly lower in BMDM^{cKO} (Fig 4 H-I). In line with hyperactivation of NFκB in BMDM^{cKO}, the secretion of TNFα was more rapidly induced upon LPS stimulation in cKO cells. This effect was toned down with time as no differences in TNFα secretion were observed 8 hours post LPS stimulation (fig 4J). These results agree with the overall inflammatory profile observed in the lungs of *Pros1*-cKO mice (Figs 2A-G, 3C), demonstrating for the first time that PROS1 is a negative regulator of the NFκB pathway in macrophages, and that the loss of PROS1 in BMDMs induces a pro-inflammatory transcriptional program.

PROS1-deletion in macrophages exacerbates lung metastasis through secreted factors.

Inflammation plays a major role in tumor progression (25, 43, 44), and loss of PROS1 in macrophages renders both BMDMs and metastasis-associated macrophages hyper-inflamed (figs 3C and fig 4), inferring that loss of PROS1 in macrophages alone may exacerbate cancer progression through cytokine secretion. We therefore tested the ability of conditioned medium (CM) collected from tumor-naïve (NT) BMDM^{cKO} to affect LLC tumor progression and metastasis. LLC cells that were educated for 24 hrs were sub-cutaneously (s.c.) injected into wild-type (WT) host mice expressing normal levels of PROS1 in all cells, to exclude host-dependent effects, and allowing any changes in LLC tumor characteristics to be attributed to their education during the incubation with CM. In this experimental setup no effect was observed on primary tumor growth, regardless of whether CM from control or cKO BMDMs was used for education (fig S5A-B). By contrast, compared to cells educated by CM-BMDM$^{fl/fl}$, LLC educated by CM-BMDM^{cKO} generated larger (0.27 ± 0.06 mm^2 versus 0.09 ± 0.02 mm^2) and more numerous (7.5 ± 1.4 versus 4.4 ± 1) metastases (fig 5 A-C). Thus, our results indicate

that BMDM^{cKO} elicit pro-metastatic features on tumor cells through secreted factors defined by a pro-inflammatory profile.

To determine whether the pro-metastatic effect of CM-BMDM^{cKO} is influenced by the tumor status of the mice, we performed a similar experiment by using BMDMs from tumor-bearing (T) mice. As for tumor-naïve CM-BMDM, no differences were observed in primary tumor growth (fig S5C-D). Conversely, LLC cells educated by CM-BMDM^{cKO} from tumor-bearing mice -but not BMDM$^{fl/fl}$ - produced significantly larger metastases (1.1 ± 0.15 mm^2 versus 0.42 ± 0.09 mm^2 (fig 5A, B). No significant effect was seen on metastasis numbers, although a trend towards increased mets was observed for CM-BMDM^{cKO} from tumor-bearing mice (fig 5C). Noticeably, BMDMs isolated from tumor-bearing mice (T) induced an overall higher metastatic burden (5A-C) demonstrating a bi-directional cross-talk between LLC and host macrophages, with PROS1 being a molecular switch of metastasis.

To elucidate whether PROS1 correspondingly functions as a molecular metastatic switch in other cancers, GFP-AT3 cells were educated (96 hrs) and subcutaneously injected into WT mice. When injected, AT3 cells have poor metastatic potential, as confirmed by our experiment: 4/8 mice educated with CM-BMDM$^{fl/fl}$ developed metastasis, which were relatively small in area (0.03 ± 0.01 mm^2). Remarkably, 7/8 mice that were injected with cells educated by CM-BMDM^{cKO} developed larger (0.1 ± 0.02 mm^2) and more numerous (2.5 ± 0.6 versus 0.87 ± 0.4; fig 5D-F) lung mets. This was also observed superficially by their GFP fluorescence and GFP protein levels in lung lysates (fig 5G-H). Akin to the LLC model, primary tumor growth was not affected in AT3 mammary breast cancer (fig S5E-F). Taken together, using two cancer models, we identify PROS1 as a novel modulator in host macrophages, shifting their cytokine secretion towards a pro-inflammatory profile, which in turn exacerbates lung and mammary tumor metastasis.

Conditioned medium of PROS1-deficient macrophages drives multiple invasive properties of tumor cells.

We next characterized the specific cellular phenotypes inflicted by CM-BMDM^{cKO} underlying the elevated metastatic burden observed in *Pros1*-cKO mice. LLC cells educated by CM from tumor-naive BMDM^{cKO} had more surviving colonies after 10 days (fig 6A-B), and superior growth in soft agar (fig 6C-D). Increased activation of oncogenic and survival pathways was observed as indicated by elevated pERK and pAKT levels in LLC cells educated by CM-BMDM^{cKO} (fig 6E-F). Similar effects were observed for AT3 cells, with the exception of unaffected pERK (fig S6A-E).

To gain insight into the metastasis-promoting molecular changes within tumor cells induced by CM-BMDM^{cKO}, we examined expression of matrix metalloproteinase 9 (MMP9), a potent extracellular matrix (ECM) degrading enzyme known to facilitate metastasis of many tumors including lung cancer (45, 46). While MMP9 levels in metastatic lungs of fl/fl mice were barely detectable, MMP9 expression was highly upregulated in metastatic cKO lungs (fig 6G-H). We further examined markers associated with the epithelial-to-mesenchymal transition (EMT) supporting migratory and invasive properties. We observed downregulation of E-cadherin, and upregulation of N-cadherin in cells educated with CM-BMDM^{cKO}, but not CM-BMDM$^{fl/fl}$, indicating cells underwent EMT. No changes were recorded for vimentin (fig 6I-J). Moreover, this EMT-related molecular switch was reflected phenotypically, as LLC educated by CM-BMDM^{cKO} had superior invasive potential (fig 6K-L).

PROS1 supplementation suppresses the pro-inflammatory profile of macrophages and restrains their pro-metastatic properties.

Our data indicate the pro-inflammatory nature of *Pros1*-deficient macrophages supports metastatic outcome. If so, we reasoned that adding exogenous PROS1 would dampen the elevated inflammation of *Pros1*-cKO BMDMs. Indeed, addition of purified

PROS1 (25nM) to LPS-stimulated cKO BMDMs reduced secretion of TNFα, IL-6 and IL-10 after 5 hrs, which persisted after 20 hrs (fig 7A-C). We next tested whether exogenous PROS1 would rescue the aggressive phenotype of LLC cells acquired during education with CM-BMDM^{cKO}. Remarkably, addition of exogenous PROS1 to cKO-BMDMs attenuated phosphorylation of both ERK and AKT in educated LLC cells (fig 7D-F). Importantly, purified PROS1 directly added to LLC or AT3 cells did not affect pERK or pAKT signaling, indicating the diminished ERK and AKT phosphorylation is not due to a direct effect of PROS1 carried over from the CM onto cancer cells (fig 7G). The reversal of oncogenic signaling in LLC cells following PROS1 rescue is further extended in-vivo, as the potential of CM-BMDM^{cKO} to induce metastasis was blunted by PROS1 addition (fig 7H-J). PROS1 addition reversed both the number and size of metastatic nodules (fig 7I,J). Altogether, addition of PROS1 is sufficient to inhibit inflammation in *Pros1*-cKO BMDMs, and to obliterate their pro-metastatic effect in-vivo through modulation of ERK and AKT oncogenic pathways.

To gain further mechanistic insight into the factors promoting metastasis secreted by cKO BMDMs, we focused on IL-10, which was prominently upregulated following *Pros1* inhibition (figs 2A-B, S2F-G, 3C, 3H and 4A-B). We first determined whether IL-10 levels are linked with the inflamed state observed in BMDM^{cKO} cells. IL-10 production was measured by ELISA following TNFα stimulation. Higher TNFα levels induced higher IL-10 secretion by both control and cKO BMDMs, with a stronger response in cKO cells (fig 7K). Akin to TNFα, LPS treatment also increased IL-10 secretion, which was inhibited in the presence of anti-TNFα neutralizing antibodies (fig 7L). Furthermore, the dynamics of *Il-10* mRNA following LPS stimulation differs between control and cKO BMDMs. An initial peak at 2 hrs post stimulation was recorded for both control and cKO cells, yet IL-10 expression was suppressed in control BMDMs, but continued to rise in *Pros1*-deficient cells, indicating the lack of a PROS1-dependent regulatory mechanism (fig 7M). Notably, this elevation in IL-10 expression was reversed in the presence of purified PROS1 (fig 7N). Thus, IL-10

expression within BMDMs can be gauged by PROS1 levels, its upregulation in cKO BMDMs is TNFα-dependent, and is linked to the inflammatory status of the cells.

The pro-metastatic potential of *Pros1*-cKO BMDMs is largely mediated by IL-10

High IL-10 expression by tumor-infiltrating macrophages was shown to correlate with advanced stages of non-small cell lung cancer (NSCLC), and associated with poor prognosis (47). We therefore hypothesized the pro-metastatic nature of cKO macrophages may be mediated via IL-10. IL-10 neutralization during the education period significantly suppressed the survival and invasive potential of LLC cells (fig 8A-D). Moreover, IL-10 blockade suppressed the phosphorylation of ERK, AKT and STAT3 in LLC cells educated by CM-BMDM^{cKO} (fig 8E-F). IL-10 neutralization also arrested the metastatic potential of LLC cells induced by education with CM-BMDM^{cKO}, without affecting CM-BMDM$^{fl/fl}$ educated cells. These effects were characterized by reduction of mets area from 0.38 ± 0.09 mm^2 for IgG-treated cKO cells to 0.087 ± 0.05 mm^2 in the presence of anti-IL-10. Similarly, mets numbers were reduced from 15.2 ± 3.1 for IgG-treated cKO cells to 4 ± 1.8 in the presence of anti-IL-10 (fig 8G-I). Taken together, the absence of PROS1 in macrophages leads to an elevated pro-inflammatory cytokine profile, including high TNFα levels, which in turn stimulate IL-10 production. IL-10 increased activation of ERK, AKT and STAT3 signaling promoting survival and invasion phenotypes observed both in-vitro and in-vivo.

Secretion of TNFα and IL-6 by macrophages is regulated by PROS1 through TAM receptors, and diverges from that of IL-10.

We previously showed that PROS1 is a cognate ligand for the TAM-Rs (42), and that PROS1 inhibits inflammation in a murine peritonitis model (16). Similarly, MERTK regulates inflammation by inhibiting TNFα secretion in macrophages (17, 48). We next tested whether the effects of PROS1 in BMDMs are mediated by MERTK. At steady state, phosphorylation of MERTK (pMERTK) in cKO BMDMs was only 42% of that in PROS1-expressing cells (fig S9A-B); indicating endogenous PROS1 is a MERTK

agonist. Addition of PROS1 to starved BMDMs increased pMERTK in $BMDM^{fl/fl}$ and $BMDM^{cKO}$, validating PROS1 as a MERTK agonist in BMDMs (fig S9C-D). Of note, addition of PROS1 to $BMDM^{fl/fl}$ stimulated pMERTK to a greater extent than in $BMDM^{cKO}$ (fig S9C-D), supporting endogenous PROS1 is a major agonist of MERTK in macrophages. Next, once verified (fig S9E-F), TAM-R kinase inhibitors were added to BMDM cultures to identify whether PROS1 effects are mediated via TAM-Rs. Akin to PROS1 reversing metastasis in-vivo (fig 7H-J), the potential of CM-$BMDM^{cKO}$ to support in-vitro invasion through matrigel was abrogated in the presence of PROS1 (Fig 9 A-B). To establish that PROS1 signal is mediated by TAM-Rs, we blocked TAM-R function using UNC4241- a small molecule pan-TAM-R kinase inhibitor. Surprisingly, UNC4241 did not interfere with the capacity of PROS1 to suppress invasion (fig 9A-B). Given that IL-10 within CM-$BMDM^{cKO}$ promotes invasion (fig 8C-D), we inspected the regulation of IL-10, TNFα and IL-6 by TAM-Rs. Whereas both UNC4241 (pan-TAM) and UNC4203 (MERTK specific) inhibitors abated the capacity of PROS1 to inhibit TNFα and IL-6 secretion, IL-10 levels were unaffected (fig 9C). These results, suggest that while PROS1 suppression of TNFα and IL-6 depends on MERTK-kinase function, the regulation of IL-10 by PROS1 may be regulated either by a non-kinase function of MERTK, or in an altogether MER-independent manner. Moreover, these results agree with the invasive property of LLC being IL-10 dependent, and the incapacity of UNC4241 to interfere with PROS1 inhibition of LLC invasion (fig 9A-B). STAT1 and SOCS3 are known downstream effectors of MERTK in various cells (14, 49). Both pSTAT1 levels and *Socs3* transcription increased following PROS1 stimulation, as expected. However, addition of UNC4203 was unable to perturb pSTAT1 or *Socs3* stimulation by PROS1 (fig 9D-F). Taken together, our data indicate that in macrophages TNFα and IL-6 are mainly regulated by MERTK kinase activity, and provide evidence for the divergence of IL-10 regulation.

PROS1 ablation in myeloid cells abrogates their T cell stimulatory potential.

We next sought to identify whether deletion of PROS1 in myeloid cells has a broader systemic effect involving additional immune cells, as immune-based anti-tumor responses within the primary and metastatic sites are known to shape tumor progression and metastases (30, 50). IL-10 secreted by macrophages elicits immune-suppression by inhibition of T cell anti-tumor responses (51, 52). We therefore reasoned that elevated secretion of IL-10 by $BMDM^{cKO}$ and lung macrophages might support metastasis through immune-suppression. We first tested the effect of macrophage-derived PROS1 on T cell proliferation within a metastatic context. For this, stimulated T cells were incubated in the presence of control or *Pros1*-cKO macrophages sorted from metastatic lungs. Compared to control macrophages, PROS1-deficient macrophages significantly inhibited T cell proliferation by 23%, revealing that cKO macrophages suppress T cell proliferation. Addition of purified PROS1 to the culture significantly rescued this suppressive capacity, suggesting a T cell stimulatory function for PROS1 (fig 10A and fig S10B). Furthermore, IL-10 neutralizing antibodies abrogated the inhibitory effect of PROS1-deficient macrophages on T cell proliferation (figs S10A and S10B), pointing to an immune-suppressive role for IL-10 following PROS1 ablation in metastatic lung macrophages. Examination of total ($CD3^+$) T cells from metastatic lungs revealed a trend towards decreased T cell numbers in cKO lungs, but similar $CD4^+$ and $CD8^+$ frequencies in both mouse models (fig 10B, C). Nitric oxide (NO) produced by macrophages is upregulated by IL-10 (53) and was shown to inhibit T cell activation (54, 55). We measured elevated nitrite levels (the product of NO decomposition) in the medium of *Pros1*-cKO macrophages sorted from metastatic lungs, which declined upon IL-10 neutralization (fig 10D).We further tested the levels of the T cell receptor ζ-chain subunit (ζ-chain) relative to CD3□□□which serves as a biomarker for an immunosuppressive environment, directly gauging T cell function (56). Compared to PROS1-proficient

mice, expression of ζ-chain was significantly downregulated in T cells from cKO metastatic lungs, indicating their impaired function in a metastatic milieu (fig 10E, F). In line with reduced ζ-chain expression, $CD8^+$ and $CD4^+$ T cells isolated from cKO mice had higher levels of the immune suppressive molecules Programmed Cell Death Protein 1 (PD1) and Cytotoxic-T-Lymphocyte-Associated-Protein-4 (CTLA4), respectively (fig 10G-J), insinuating induced T cell immunosuppression in metastatic lungs of cKO mice. Collectively, our data reveal that PROS1 stimulates T cell proliferation directly and indirectly by inhibition of IL-10 production within macrophages. Additionally, reduced ζ-chain and elevated immune checkpoint inhibitors indicate effects on T cell activation following a myeloid-specific PROS1 deletion within the metastatic niche.

Our results pointing at a possible immunosuppressive state of T cells in *Pros1*-cKO tumor-bearing mice could also be due to sub-optimal stimulation by DCs, as tumor-infiltrating DCs expressing $CD11c^+MHC\text{-}II^+$ limit tumor progression through T cell activation (57). To test whether PROS1-cKO DCs possess decreased T cell stimulatory potential, we generated bone marrow-derived DCs (BMDCs) from control and cKO mice. Compared to BMDMs, LysM-Cre efficiency was reported to be less effective in BMDCs, reaching 31% (22). The overall knockout efficiency in our BMDC culture reached 47%, yet in stark contrast to BMDMs, no changes were reported for tumor-modulating cytokines such as *Tgfb*, *Ifng*, *Gmcsf*, *Il-12p35* or *Il-10* (fig 11A). Although similar frequencies of $CD45^+CD11c^+$ cells were obtained, the BMDC population expressing $MHC\text{-}II^{hi}$ was significantly reduced in cKO mice (fig 11B-C). Moreover, $CD11c^+MHC\text{-}II^{hi}$ cells expressed less of the CD40 co-stimulatory molecule (fig 11D, E), suggesting their impaired ability to stimulate T cells. Analyzing DCs from metastatic lungs (fig 11F-I), we found a trend towards a reduction in the $CD11c^+MHC\text{-}II^{hi}$ population in cKO lungs (fig 11F, G), suggesting their attenuated potential to stimulate T cells in situ. This is supported by their reduced expression of CD40 and CD86 co-

stimulatory molecules (fig 11H, I), implying impaired T cell stimulatory potential in a metastatic environment. Taken together, our results indicate that inhibition of PROS1 in myeloid cells leads to a broad immune suppressive phenotype involving macrophages, DCs and T cells, with PROS1 acting both as a regulator of inflammation within macrophages, and affecting T cell proliferation directly, and indirectly via suppression of IL-10.

Discussion

Bone marrow-derived immune cells contribute to tumor angiogenesis, invasion and metastasis (2, 3, 30, 58, 59), but the signaling mechanisms underlying these processes have not been fully elucidated. The metastasis-promoting functions of immune cells were shown to be driven by numerous molecules, some of which are FLT-1 (VEGF-R1), CARD9 and MMP9 (60–63). Yet, macrophage-derived proteins possessing anti-metastatic qualities are sparse. Here, we identify a metastatic-inhibitory role for PROS1 expressed by bone marrow-derived circulating myeloid cells. Acting as a molecular switch of inflammation, the ablation of PROS1 from this subset of immune cells increases tumor metastatic efficiency in both lung and mammary cancer models. We further reveal that inhibiting PROS1 expression by metastasis-associated macrophages promotes immune evasion by modulating antitumor responses within T cells, and highlight a key role for IL-10 in both directly promoting tumor cell invasion and immune suppression.

Our data show that primary tumor growth is unaffected by PROS1 expressed by circulating myeloid cells (fig 1, fig S1, fig S5). While our in-vitro analyses indicate education with *Pros1*-cKO BMDMs increased aggressiveness of both LLC and AT3 cells (figs 6, S6), these cells did not generate larger primary tumors (fig S5), and PROS1 expression in myeloid cells had no effect on their tumor infiltration (fig S2A, B). Rather, the education by *Pros1*-deficient BMDMs embodied in enhanced metastasis (fig 5),

indicating different requirements and conditions dictate the impact of myeloid cells on primary tumor versus metastatic loci. In alignment with our results, inhibition of FLT1 kinase activity in host macrophages neither affected macrophage recruitment into metastatic lesions nor to the primary tumor, but instead regulated expression of inflammatory genes in macrophages, promoting metastasis (61). Similarly, toll-like receptor 2 (TLR2) supports lung metastasis of LLC, without affecting primary tumor growth (7). Together with these studies, our data point at distinct behaviors for metastatic and primary tumor cells, which may stem from the increased permissiveness and/or synergism provided by the lungs, but not at the primary tumor site. Indeed, primary and metastatic sites differ both genetically (64) and immunologically (65, 66). Given that tumor cells are affected by interactions with immune cells, the differences in immune cell infiltration observed (fig 2 D-G and fig S2 A, B) generate distinct immune landscapes in primary and metastatic sites, which in turn may generate environments with differential permissiveness for cancer cell growth. This is supported by elevated MMP9 expression in lungs of cKO mice, but not of controls (fig 6 G, H).

We find that PROS1 functions as a negative regulator of inflammation in macrophages (figs 4, 7), in a MERTK-dependent manner (figs 9 and S9), and that PROS1 neutralization leads to enhanced tissue inflammation and consequently increased metastatic seeding (figs 2, S2). Ablation of PROS1 within BMDMs led to their pro-inflammatory cytokine signature, mediated through NFκB (fig 4). This pathway is also inhibited by PROS1 in dendritic cells (DCs) (14), through activation of TAM-R signaling. Inactivation of TAM-Rs (TAMR) in mice led to a hyperactive immune state with an increased inflammatory cytokine signature (20, 67). TAMRs inhibit inflammation by several mechanisms (11, 13), one of which being the phagocytic uptake of apoptotic cells (11, 68). Apoptotic cell clearance not only eliminates further inflammation by secondary necrosis of uncleared dying cells (18, 69) but also actively stimulates anti-inflammatory signaling (14, 15, 70, 71). Within macrophages, MERTK attenuates inflammatory signaling (17), and we recently showed that macrophage-derived PROS1

contributes both to their uptake of apoptotic cells and to dissipating inflammatory cytokine expression in a model of zymosan -induced peritonitis (16).

Along with increased expression of pro-inflammatory cytokines, PROS1 ablation led to elevated expression of IL-10, a wound healing cytokine, also upregulated in macrophages following LPS stimulation to regulate the extent of inflammation and resulting tissue damage (72, 73). IL-10 is also known for its immunosuppressive capacities (51, 74, 75), and was recently shown to induce invasion of gastric cancer cells (76). We find that IL-10 secreted by *Pros1*-deficient BMDMs and metastasis-associated macrophages directly contributes to metastatic progression by inducing LLC invasiveness and survival (fig 8) and promoting immune-suppression by inhibiting T cell proliferation (fig 10). In terms of PROS1-TAMR signaling within macrophages, lack of TYRO3 expression in BMDMs implies MERTK as the dominant PROS1 receptor (48). Accordingly, MERTK phosphorylation is significantly reduced in *Pros1*-cKO macrophages (fig S9). Nevertheless, inhibition of MERTK kinase activity reveals a disparity between PROS1 mediated regulation of TNFα and IL-6 to that of IL-10, which is unchanged in the presence of MERTK kinase inhibitors (fig 9C). This deflection may provide a mechanistic basis for the diverse outcomes observed when different TAM components are inhibited, and is consistent with the inability of TAMR kinase inhibitors to block the effect of PROS1 on LLC invasion (fig 9A-B), which we find is driven by IL-10 (fig 8). In vivo, this may be reflected by different TME landscapes dynamically driving distinct molecular pathways. We previously assessed the role of PROS1 in the resolution of inflammation following zymosan A-induced peritonitis (16), where secretion of IL-10 by peritoneal resolution-phase cKO macrophages was lower than in fl/fl controls at baseline and after LPS stimulation. Yet, addition of PROS1 suppressed IL-10 production (16). Thus, we propose the effect of PROS1 on IL-10 expression is context-dependent. A potential factor which may modulate the IL-10 response is TNFα, necessary for IL-10 expression in inflammatory macrophages (fig 7K-L). At the same time, TNFα is regulated by the PROS1-MERTK axis (fig 9C), thus multiple context-dependent factors regulate

IL-10 production. Moreover, while PROS1 inhibits LPS-induced IL-10 expression in BMDMs (this study), GAS6 upregulation was reported to enhance IL-10 production under similar conditions (77), in which Pros1 expression was unchanged. Taken together, the regulation of IL-10 by TAM signaling is likely to depend on the functional ligand-receptor interactions at a given physiological context. Further investigations are necessary to elucidate IL-10 regulation by PROS1, including non-kinase functions of MERTK and heterodimers with non-TAM receptors (14).

We reveal multiple immunoregulatory roles for PROS1 secreted by metastasis-associated macrophages. In addition to regulating the expression of the immunosuppressive cytokine IL-10 as mentioned above, PROS1 significantly rescued the inhibitory nature of cKO macrophages (fig 10A), suggesting that PROS1 stimulates mouse T cells. Indeed, recent studies revealed PROS1 stimulates human $CD4^+$ (78) and $CD8^+$ T cells (79). Moreover, neutralizing IL-10 experiments suggest that PROS1 promotes T cell proliferation through IL-10 suppression (fig 10A). Next, we show that PROS1 constrains immune suppression in the TME, as tumor-resident T cells from cKO mice had downregulated □-chain expression, and higher PD1 and CTLA4 expression (fig 10). Similarly, inhibiting PROS1 within DCs led to a reduction in maturation and costimulatory molecules (fig 11), suggesting impaired T cell activation by DCs and further contributing to an immune-suppressive environment. Using a mouse platform, this study is the first to show that in a tumor-related context, PROS1 supports multiple aspects of immune activation, a feature which may be exploited to increase antitumor immune responses.

In addition to their role as negative regulators of inflammation, TAMRs are also active proto-oncogenes, where their overexpression stimulates proliferation, migration, cell survival and resistance to chemotherapy in numerous human cancers (9), pointing to TAMRs as attractive targets for anti-cancer treatment (80–82). As drivers of oncogenesis, both TAMR ligands GAS6 and PROS1 were shown to stimulate TAM oncogenic signaling within tumor cells (10, 83). We previously identified the upregulation

of GAS6 by tumor-infiltrating macrophages following education by tumor cells, which in turn fueled tumor growth and metastasis (8). Thus, tumor infiltrating BM-derived immune cells are educated by tumor cells to upregulate the TAMR agonist GAS6, facilitating primary and metastatic growth. Interestingly, PROS1 was not upregulated in these infiltrating tumor macrophages (8). Our present study surprisingly shows that unlike its functional homologue GAS6, PROS1 expression in host macrophages has no effect on LLC and AT3 primary tumor growth (figs 1, S1 and S5). Unexpectedly, we find the effect of PROS1 expression by host macrophages on metastasis was opposite to that of GAS6: metastasis was exacerbated by PROS1 ablation, but alleviated by GAS6-deficiency in bone-marrow derived cells. These findings reveal contending roles for the TAMR ligands PROS1 and GAS6 within the TME. Varying outcomes were also observed following ablation of different TAMRs in the various tumor models tested (11). Reduced tumor growth and metastasis was reported following MERTK inhibition in BM-derived cells in various tumor models, despite their pro-inflammatory signature (84). This can be explained by the fact that GAS6 upregulation was prevented in MERTK-deficient BM-derived cells, or by the observed lack of MERTK-mediated suppression of antitumor immunity (84). Consistent with our observation, loss of both AXL and MERTK in intestinal resident macrophages led to a pro-inflammatory milieu, favoring a tumor-promoting environment (85). Taken together, our results show that PROS1 expression in bone marrow derived macrophages potently protects from lung metastasis by inhibiting inflammation.

The effect of BMDM-derived PROS1 on tumor cells did not require direct contact between tumor infiltrating macrophages and tumor cells. This was demonstrated by efficient metastatic seeding when LLC cells were injected into the tail vein of *Pros1*-cKO mice, bypassing the primary tumor (fig S2 C-E). It is possible that PROS1-deficient macrophages preferentially migrate to the prospective metastatic sites, where they support and nurture the lungs as a preferred site for future metastasis. This is supported by our BM-transplantation experiments, which indicate that BM-derived circulating cells

modulate lung inflammation (fig 3D-E), and suggests that inflammation is a prerequisite for metastatic colonization of the lungs by LLC and AT-3 cells. Similarly, Qian et. al. identified a CCR2 and Gr1-positive distinct population of inflammatory monocytes which are preferentially recruited to metastatic sites over primary tumors, where they promote extravasation of tumor cells into lung parenchyma (33, 34).

Regarding PROS1 functions in cancer, this study reveals its functional diversity, which may be context-dependent. We previously showed that PROS1 stimulates ERK and AKT phosphorylation in oral squamous cell carcinoma (OSCC), contributing to enhanced tumor cell proliferation and migration (10). In contrast to OSCC tumor cells, here we show the addition of exogenous PROS1 (25nM) does not stimulate ERK and AKT phosphorylation within LLC and AT-3 cells (fig 7G). Rather, when added to BMDMs, PROS1 dampened NFkB-mediated inflammatory cytokine production (figs 7 A-C, 9C), which in-turn attenuated ERK and AKT activation within LLC cells (fig 7D-F). Our results point to the PROS1/IL-10 axis in macrophages as a novel pathway where PROS1 directly influences tumor cell survival and invasive potential (fig. 8). Thus, although BMDM-derived PROS1 may potentially stimulate oncogenic pathways in tumor cells via direct TAMR activation, it seems the dominant route of tumor cell activation in LLC and AT3 models occurs via inflammation, with IL-10 being a key mediator stimulating ERK, ATK and STAT3 and facilitating invasion, survival and metastasis (fig 8).

Interestingly, tumor-derived PROS1 was recently reported to suppress the immune response in a melanoma model, where its expression affected immune cell infiltration and primary tumor growth (86). Primary tumor growth and its infiltration by immune cells in both lung and mammary models were not affected by PROS1 expression within myeloid cells, suggesting PROS1-dependent TME responses may vary between tumors. Alternatively, altered biochemical and biological responses may result from different PROS1 variants expressed by tumor and immune cells.

Within BMDMs, PROS1 is a negative regulator of the NFkB pathway, affecting the secretion of TNFα and IL-6 (figs 2A-C, 4 and 9C). Elevated expression of these

cytokines by BMDMs was previously shown to be stimulated by versican, identifying this proteoglycan secreted by LLC cells as a tumor-secreted factor rendering BMDMs pro-metastatic (7). Our data suggest that loss of PROS1 expression within BMDMs may be sufficient to bypass this versican-dependent pro-metastatic effect. The presence of exogenous PROS1 to $BMDM^{cKO}$ was sufficient to rescue the metastatic phenotype – reversing metastasis to baseline levels observed in control mice (fig 7), pointing to BMDM treatment with PROS1 as a putative therapeutic strategy.

In summary, our findings suggest that PROS1 is a key regulator of macrophage inflammatory signaling, also affecting various aspects of immune activation, which together have a strong impact on metastasis. PROS1 expression within macrophages attenuates NFkB-mediated expression of TNFα and IL-6 in a TAM-dependent manner, induces antitumor immunity both directly and via IL-10, affecting metastatic outcome. IL-10 is revealed as a key cytokine promoting LLC survival and invasiveness as well as immune suppression, and its regulation by PROS1 does not require MERTK kinase activity. The role PROS1 takes in macrophages during inflammation dominates its potential role as a ligand for the proto-oncogenic TAM-Rs, in contrast to what has been previously described for GAS6. Finally, our data provide a strong rationale for utilizing PROS1 to suppress inflammation and stimulate anti-tumor immunity to restrict metastasis.

Methods

Detailed experimental methods are provided in THE ONLINE Supplement.

Study Approval

All animal studies were approved by the institutional animal care and use committee (IACUC) –approval # MD-14025-5. Veterinary care was provided to all animals by the Hebrew University animal care facility staff in accordance with AAALAC standard procedures under specific pathogen-free conditions.

Author contributions

AM and TBC designed experiments, AM, VLY, KBM, AH, ZT, GM, M Berger, SP performed experiments, AM, AH, SMZ and TBC analyzed data, M Berger, M Baniyash and SL provided imperative advice in designing experiments and provided critical insight. TBC wrote the manuscript. All authors approved the manuscript.

Acknowledgments

This study was supported by a Research Career Development Award (RCDA) and by a Project Grant from the Israel Cancer Research Fund (ICRF) to TBC, a research grant by the Israel Cancer Association (ICA) and funded by the Golombo Foundation to TBC, and an ICRF Booster grant to AM. Dr. Loges is funded by a Heisenberg professorship (LO1863/4-1) and by the ubone SPP program (LO1863/5-1) awarded by the German Research Council. Furthermore, she receives funding from the Margarete-Clemens Stfitung. We thank Nikita Gvardiyan and Shira Kaikov for technical support, Yaara Tabib, Dr. Oded Hayman, Noam Koren and Prof. Avi-Hai Hovav for assisting with FACS experiments and analysis. We also thank Hadas Masuri and Zhanna Yekhtin for experimental support and Dr. Zvi Granot for providing cancer cell lines. We thank Prof. Baniyash for kindly providing the anti-□-chain antibody, and Prof. Xiaodong Wang, University of North Carolina, for providing the anti-TAM inhibitors.

References:

1. Hao NB et al. Macrophages in tumor microenvironments and the progression of tumors. *Clin. Dev. Immunol.* 2012;2012. doi:10.1155/2012/948098

2. Qian BZ, Pollard JW. Macrophage Diversity Enhances Tumor Progression and Metastasis. *Cell* 2010;141(1):39–51.

3. Quail DF, Joyce JA. Microenvironmental regulation of tumor progression and metastasis. *Nat. Med.* 2013;19(11):1423–1437.

4. Pollard JW. Tumour-educated macrophages promote tumour progression and metastasis. *Nat. Rev. Cancer* 2004;4(1):71–78.

5. Quaranta V, Schmid MC. Macrophage-Mediated Subversion of Anti-Tumour Immunity. *Cells* 2019;8(7):747.

6. Colegio OR et al. Functional polarization of tumour-associated macrophages by tumour-derived lactic acid. *Nature* 2014;513(7519):559–563.

7. Kim S et al. Carcinoma-produced factors activate myeloid cells through TLR2 to stimulate metastasis. *Nature* 2009;457(7225):102–106.

8. Loges S et al. Malignant cells fuel tumor growth by educating infiltrating leukocytes to produce the mitogen Gas6. *Blood* 2010;115(11):2264–2273.

9. Graham DK, Deryckere D, Davies KD, Earp HS. The TAM family: Phosphatidylserine-sensing receptor tyrosine kinases gone awry in cancer. *Nat. Rev. Cancer* 2014;14(12):769–785.

10. Abboud-Jarrous G et al. Protein S drives oral squamous cell carcinoma tumorigenicity through regulation of AXL. *Oncotarget* 2017;8(8):13986–14002.

11. Burstyn-Cohen T, Maimon A. TAM receptors, phosphatidylserine, inflammation, and cancer. *Cell Commun. Signal.* 2019;17(1):156–165.

12. Lemke G, Rothlin C V. Immunobiology of the TAM receptors. *Nat Rev Immunol* 2008;8(5):327–336.

13. Rothlin C V., Carrera-Silva EA, Bosurgi L, Ghosh S. TAM receptor signaling in immune homeostasis. *Annu. Rev. Immunol.* 2015;33:355–391.

14. Rothlin C V., Ghosh S, Zuniga EI, Oldstone MBA, Lemke G. TAM Receptors Are Pleiotropic Inhibitors of the Innate Immune Response. *Cell* 2007;131(6):1124–1136.

15. Carrera-Silva EA et al. T Cell-Derived Protein S Engages TAM Receptor Signaling in Dendritic Cells to Control the Magnitude of the Immune Response. *Immunity* 2013;39(1):160–170.

16. Lumbroso D et al. Macrophage-derived protein S facilitates apoptotic polymorphonuclear cell clearance by resolution phase macrophages and supports their reprogramming. *Front. Immunol.* 2018;9:358.

17. Camenisch TD, Koller BH, Earp HS, Matsushima GK. A novel receptor tyrosine kinase, Mer, inhibits TNF-alpha production and lipopolysaccharide-induced endotoxic shock. *J. Immunol.* 1999;162(6):3498–503.

18. Cohen PL et al. Delayed apoptotic cell clearance and lupus-like autoimmunity in mice lacking the c-mer membrane tyrosine kinase. *J. Exp. Med.* 2002;196(1):135–140.

19. Sen P et al. Apoptotic cells induce Mer tyrosine kinase-dependent blockade of NF-κB activation in dendritic cells. *Blood* 2007;109(2):653–660.

20. Lu Q, Lemke G. Homeostatic regulation of the immune system by receptor tyrosine kinases of the Tyro 3 family. *Science* 2001;293(5528):306–311.

21. Burstyn-Cohen T, Heeb MJ, Lemke G. Lack of Protein S in mice causes embryonic lethal coagulopathy and vascular dysgenesis. *J. Clin. Invest.* 2009;119(10):2942–2953.

22. Clausen BE, Burkhardt C, Reith W, Renkawitz R, Förster I. Conditional gene targeting in macrophages and granulocytes using LysMcre mice. *Transgenic Res.* 1999;8(4):265–277.

23. Weiss L, Ward PM. Lymphogenous and hematogenous metastasis of Lewis lung carcinoma in the mouse. *Int. J. Cancer* 1987;40(4):570–574.

24. Pikarsky E et al. NFκB functions as a tumour promoter in inflammation-associated cancer. *Nature* 2004;431(7007):461–466.

25. Ben-Neriah Y, Karin M. Inflammation meets cancer, with NF-kappaB as the matchmaker. *Nat. Immunol.* 2011;12(8):715–723.

26. Karin M. Nuclear factor-kappa B in cancer development and progression. *Nature* 2006;441(7092):431–436.

27. Hussell T, Bell TJ. Alveolar macrophages: Plasticity in a tissue-specific context. *Nat. Rev. Immunol.* 2014;14(2):81–93.

28. Bedoret D et al. Lung interstitial macrophages alter dendritic cell functions to prevent airway allergy in mice. *J. Clin. Invest.* 2009;119(12):3723–3738.

29. Tan SYS, Krasnow MA. Developmental origin of lung macrophage diversity. *Dev.* 2016;143(8):1318–1327.

30. Joyce JA, Pollard JW. Microenvironmental regulation of metastasis. *Nat. Rev. Cancer* 2009;9(4):239–252.

31. Gorelik E, Wiltrout RH, Brunda MJ, Holden HT, Herberman RB. Augmentation of metastasis formation by thioglycollate-elicited macrophages. *Int. J. Cancer* 1982;29(5):575–581.

32. Nowicki A et al. Impaired tumor growth in colony-stimulating factor 1 (CSF-1)-deficient, macrophage-deficient op/op mouse: Evidence for a role of CSF-1-dependent macrophages in formation of tumor stroma. *Int. J. Cancer* 1996;65(1):112–119.

33. Qian BZ et al. CCL2 recruits inflammatory monocytes to facilitate breast-tumour metastasis. *Nature* 2011;475(7355):222–225.

34. Qian B et al. A distinct macrophage population mediates metastatic breast cancer cell extravasation, establishment and growth. *PLoS One* 2009;4(8):e6562.

35. Lin EY, Nguyen A V., Russell RG, Pollard JW. Colony-stimulating factor 1 promotes progression of mammary tumors to malignancy. *J. Exp. Med.* 2001;193(6):727–739.

36. Shand FHW et al. Tracking of intertissue migration reveals the origins of tumor-infiltrating monocytes. *Proc. Natl. Acad. Sci. USA.* 2014;111(21):7771–7776.

37. Sharma SK et al. Pulmonary Alveolar Macrophages Contribute to the Premetastatic Niche by Suppressing Antitumor T Cell Responses in the Lungs. *J. Immunol.* 2015;194(11):5529–5538.

38. Kratofil RM, Kubes P, Deniset JF. Monocyte conversion during inflammation and injury. *Arterioscler. Thromb. Vasc. Biol.* 2017;37(1):35–42.

39. Matute-Bello G et al. Optimal timing to repopulation of resident alveolar macrophages with donor cells following total body irradiation and bone marrow transplantation in mice. *J. Immunol. Methods* 2004;292(1–2):25–34.

40. Deng T, Zhang Y, Chen Q, Yan K, Han D. Toll-like receptor-mediated inhibition of Gas6 and ProS expression facilitates inflammatory cytokine production in mouse macrophages. *Immunology* 2012;135(1):40–50.

41. Van Der Meer JHM, Van Der Poll T, Van't Veer C. TAM receptors, Gas6, and protein S: Roles in inflammation and hemostasis. *Blood* 2014;123(16):2460–2469.

42. Burstyn-Cohen T et al. Genetic Dissection of TAM Receptor-Ligand Interaction in Retinal Pigment Epithelial Cell Phagocytosis. *Neuron* 2012;76(6):1123–1132.

43. Mantovani A, Allavena P, Sica A, Balkwill F. Cancer-related inflammation. *Nature* 2008;454(7203):436–444.

44. Coussens LM, Werb Z. Inflammation and cancer. *Nature* 2002;420(6917):860–867.

45. Merchant N et al. Matrix metalloproteinases: Their functional role in lung cancer. *Carcinogenesis* 2017;38(8):766–780.

46. Chou CH et al. MMP-9 from sublethally irradiated tumor promotes Lewis lung carcinoma cell invasiveness and pulmonary metastasis. *Oncogene* 2012;31(4):458–468.

47. Zeni E et al. Macrophage expression of interleukin-10 is a prognostic factor in nonsmall cell lung cancer. *Eur. Respir. J.* 2007;30(4):627–632.

48. Zagórska A, Través PG, Lew ED, Dransfield I, Lemke G. Diversification of TAM receptor tyrosine kinase function. *Nat. Immunol.* 2014;15(10):920–928.

49. Lee Y-J et al. Inhibiting Mer receptor tyrosine kinase suppresses STAT1, SOCS1/3, and NF-κB activation and enhances inflammatory responses in lipopolysaccharide-induced acute lung injury. *J. Leukoc. Biol.* 2012;91(6):921–932.

50. Noy R, Pollard JW. Tumor-Associated Macrophages: From Mechanisms to Therapy. *Immunity* 2014;41(1):49–61.

51. Vukmanovic S et al. T-cell activation is enhanced by targeting IL-10 cytokine production in toll-like receptor- stimulated macrophages. *ImmunoTargets Ther.* 2012;1:13.

52. Sharma S et al. T cell-derived IL-10 promotes lung cancer growth by suppressing both T cell and APC function. *J. Immunol.* 1999;163(9):5020–8.

53. Jacobs F et al. IL-10 up-regulates nitric oxide (NO) synthesis by lipopolysaccharide (LPS)-activated macrophages: Improved control of Trypanosoma cruzi infection. *Clin.*

Exp. Immunol. 1998;113(1):59–64.

54. Sato K et al. Nitric oxide plays a critical role in suppression of T-cell proliferation by mesenchymal stem cells. *Blood* 2007;109(1):228–234.

55. Ridnour LA et al. NOS inhibition modulates immune polarization and improves radiation-induced tumor growth delay. *Cancer Res.* 2015;75(14):2788–2799.

56. Baniyash M. TCR ζ-chain downregulation: Curtailing an excessive inflammatory immune response. *Nat. Rev. Immunol.* 2004;4(9):675–687.

57. Preynat-Seauve O et al. Tumor-Infiltrating Dendritic Cells Are Potent Antigen-Presenting Cells Able to Activate T Cells and Mediate Tumor Rejection. *J. Immunol.* 2006;176(1):61–67.

58. Kaplan RN, Rafii S, Lyden D. Preparing the “soil”: The premetastatic niche. *Cancer Res.* 2006;66(23):11089–11093.

59. Hanna RN et al. Patrolling monocytes control tumor metastasis to the lung. *Science* 2015;350(6263):985–990.

60. Kaplan RN et al. VEGFR1-positive haematopoietic bone marrow progenitors initiate the pre-metastatic niche. *Nature* 2005;438(7069):820–827.

61. Qian BZ et al. FLT1 signaling in metastasis-associated macrophages activates an inflammatory signature that promotes breast cancer metastasis. *J. Exp. Med.* 2015;212(9):1433–1448.

62. Hiratsuka S et al. MMP9 induction by vascular endothelial growth factor receptor-1 is involved in lung-specific metastasis. *Cancer Cell* 2002;2(4):289–300.

63. Yang M et al. Tumor cell-activated CARD9 signaling contributes to metastasis-associated macrophage polarization. *Cell Death Differ.* 2014;21(8):1290–1302.

64. Wu J et al. Genetic differences between primary and metastatic tumors from cross-institutional data. *J. Clin. Oncol.* 2018;36(15 suppl):e18572–e18572.

65. Szekely B et al. Immunological differences between primary and metastatic breast cancer. *Ann. Oncol.* 2018;29(11):2232–2239.

66. Kim R et al. Differences in tumor microenvironments between primary lung tumors and brain metastases in lung cancer patients: Therapeutic implications for immune checkpoint inhibitors 11 Medical and Health Sciences 1112 Oncology and Carcinogenesis. *BMC Cancer* 2019;19(1):19.

67. Lemke G, Lu Q. Macrophage regulation by Tyro 3 family receptors. *Curr. Opin. Immunol.* 2003;15(1):31–36.

68. Lemke G, Burstyn-Cohen T. TAM receptors and the clearance of apoptotic cells. *Ann. N. Y. Acad. Sci.* 2010;1209(1):23–29.

69. Elliott MR, Ravichandran KS. Clearance of apoptotic cells: implications in health and disease. *J. Cell Biol.* 2010;189(7):1059–70.

70. Lee CS et al. Boosting Apoptotic Cell Clearance by Colonic Epithelial Cells Attenuates Inflammation In Vivo. *Immunity* 2016;44(4):807–820.

71. Fadok VA et al. Macrophages that have ingested apoptotic cells in vitro inhibit

proinflammatory cytokine production through autocrine/paracrine mechanisms involving TGF-β, PGE2, and PAF. *J. Clin. Invest.* 1998;101(4):890–898.

72. Pengal RA et al. Lipopolysaccharide-induced production of interleukin-10 is promoted by the serine/threonine kinase Akt. *Mol. Immunol.* 2006;43(10):1557–1564.

73. Ernst O et al. Exclusive Temporal Stimulation of IL-10 Expression in LPS-Stimulated Mouse Macrophages by cAMP Inducers and Type I Interferons. *Front. Immunol.* 2019;10(1788):1788.

74. Mittal SK, Roche PA. Suppression of antigen presentation by IL-10. *Curr. Opin. Immunol.* 2015;34:22–27.

75. Jung K et al. Ly6Clo monocytes drive immunosuppression and confer resistance to anti-VEGFR2 cancer therapy. *J. Clin. Invest.* 2017;127(8):3039–3051.

76. Chen L et al. IL-10 secreted by cancer-associated macrophages regulates proliferation and invasion in gastric cancer cells via c-Met/STAT3 signaling. *Oncol. Rep.* 2019;42(2):595–604.

77. Kim SY et al. Liver X receptor and STAT1 cooperate downstream of Gas6/Mer to induce anti-inflammatory arginase 2 expression in macrophages. *Sci. Rep.* 2016;6(1):1–16.

78. Cabezo´n R et al. MERTK as negative regulator of human T cell activation. *J. Leukoc. Biol.* 2015;97(4):751–760.

79. Peeters MJW et al. MERTK Acts as a costimulatory receptor on human cd8 t cells. *Cancer Immunol. Res.* 2019;7(9):1472–1484.

80. Sheridan C. First Axl inhibitor enters clinical trials.. *Nat. Biotechnol.* 2013;31(9):775–776.

81. Verma A, Warner SL, Vankayalapati H, Bearss DJ, Sharma S. Targeting Axl and Mer kinases in cancer. *Mol. Cancer Ther.* 2011;10(10):1763–1773.

82. Schlegel J et al. MERTK receptor tyrosine kinase is a therapeutic target in melanoma. *J. Clin. Invest.* 2013;123(5):2257–2267.

83. Shiozawa Y et al. GAS6/AXL axis regulates prostate cancer invasion, proliferation, and survival in the bone marrow niche. *Neoplasia* 2010;12(2):116–127.

84. Cook RS et al. MerTK inhibition in tumor leukocytes decreases tumor growth and metastasis. *J. Clin. Invest.* 2013;123(8):3231–3242.

85. Bosurgi L et al. Paradoxical role of the proto-oncogene Axl and Mer receptor tyrosine kinases in colon cancer. *Proc. Natl. Acad. Sci.* 2013;110(32):13091–13096.

86. Ubil E et al. Tumor-secreted Pros1 inhibits macrophage M1 polarization to reduce antitumor immune response. *J. Clin. Invest.* 2018;128(6):2356–2369.

Maimon et al – Figure 1

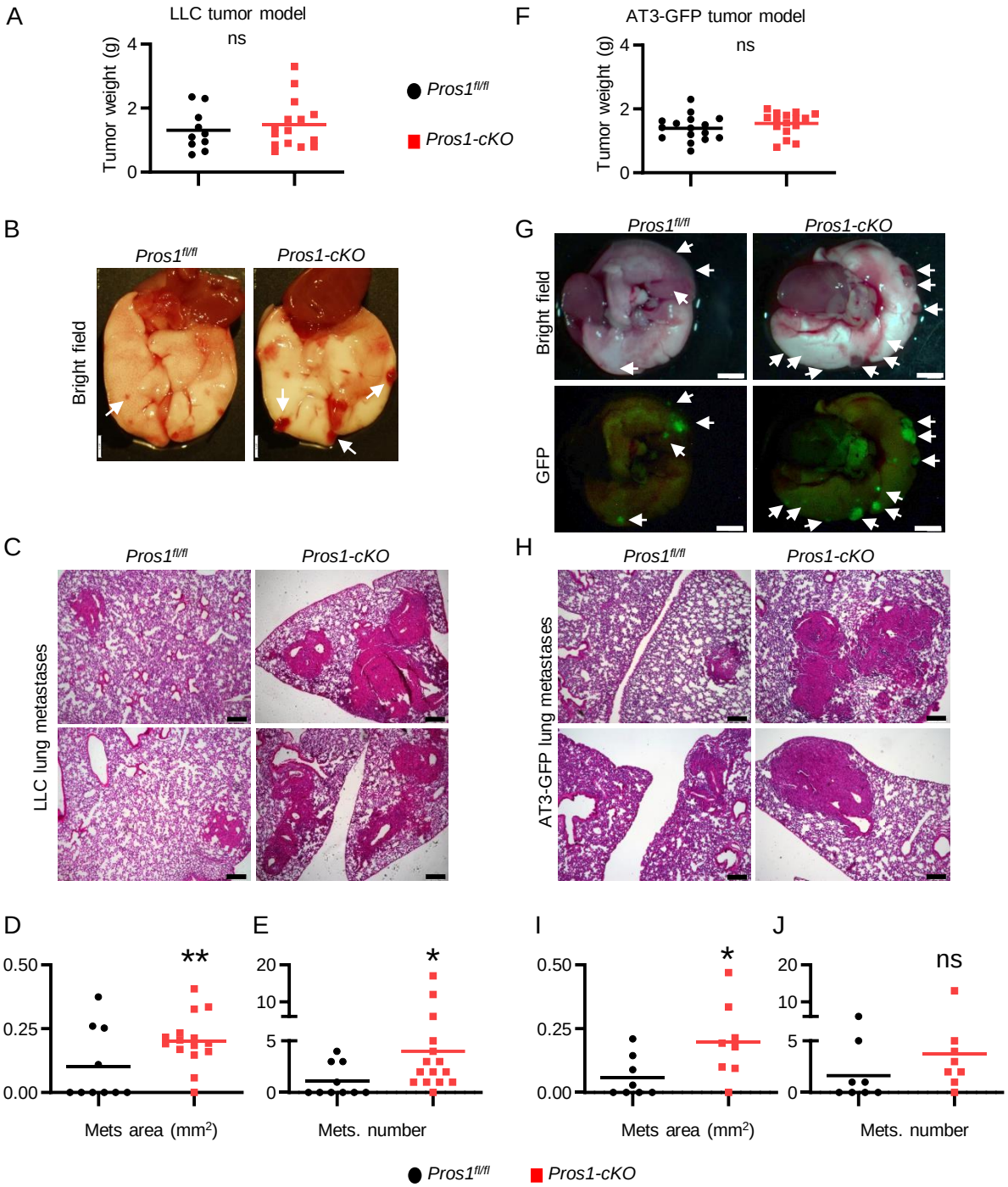

Fig.1: Genetic ablation of *Pros1* in host myeloid cells enhances metastasis.

Analysis of LLC (A-E) and AT3-GFP mammary (F-J) primary tumors and metastasis. (A, F) End-stage tumor weight (n=10, 15 mice/group in A; n=16 in F. The horizontal line marks the mean tumor weight. (B, G) Lungs Isolated three weeks after subcutaneous inoculation of $5x10^5$ LLC cells (B) or after orthotropic injection of $1x10^6$ AT3-GFP cells into each of 2 mammary glands (G). Metastatic foci appear as red nodules (arrows in B, G). GFP-expressing AT3 metastatic foci appear green under fluorescent light (G, lower panels). Scale=2mm. (C, H) Representative images of Hematoxylin & Eosin (H&E) stained sections from lungs described in B and G, respectively. Scale=200µm. (D-J) Mean area (D, I) and number (E, J) of metastasis scored. P=0.006 and 0.03 for D, E and 0.019 for I and J, respectively; t-test. ns = non-significant.

Maimon et al – Figure 2

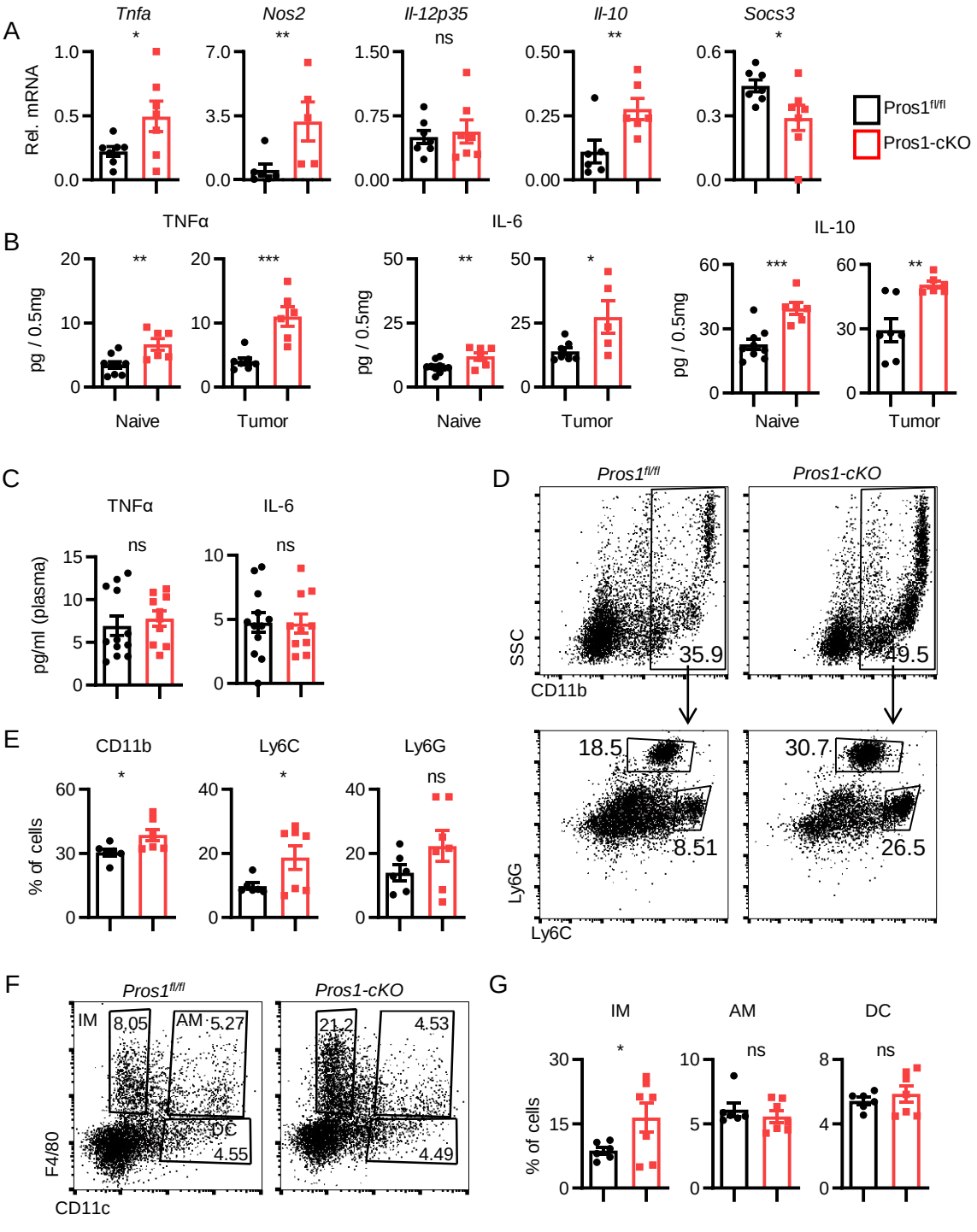

Fig.2: Characterization of lung inflammation in control and *Pros1*-cKO mice.

(A-B) An elevated inflammatory signature is present in the lungs of mice following myeloid-specific ablation of *Pros1*. (A) Relative mRNA expression, measured by RT-qPCR, of the indicated cytokines from lungs of tumor-naive *Pros1*$^{fl/fl}$ (black bars) and *Pros1*-cKO (red bars) mice. Mean ± SEM, n=5-7 mice/group; 3 independent experiments. *P≤0.02; **P≤0.01; t-test. (B) Cytokines measured by ELISA from tumor-naïve and tumor-bearing lung lysates. Mean ± SEM; n=5-10 mice/group. P values for TNFα, IL-6 and IL-10 are 0.002, 0.009, 0.0003 and P=0.0004, 0.016, 0.002 for naïve and tumor bearing lungs, respectively; t-test. (C) ELISA measurements of TNFα and IL-6 serum levels in control and cKO mice. Mean ± SEM; n=10-12 mice/group. (D-G) FACS analysis of immune cell infiltration into the lungs of tumor-naïve control and cKO mice. Representative plots (D) and quantification (E) of CD11b^{+} from CD45^{+}gated cells (top), further analyzed for Ly6G^{+}/Ly6C^{lo} (granulocytes) and Ly6G^{-}/Ly6C^{hi} (monocytes). N=7 mice/genotype; P=0.01, 0.02 for CD11b^{+} and Ly6G^{-}/Ly6C^{hi}, respectively; t-test. (F) Representative FACS plots (F) and quantification (G) of CD45^{+} gated cells stained for F4/80 and CD11c identifying three myeloid sub-populations; IM (F4/80^{+}), AM (F4/80^{+}/CD11c^{+}) and DC (CD11c^{+}). Mean percent ± SEM; n=6-7 mice/group. P=0.03 for IM.; t-test. ns = non-significant.

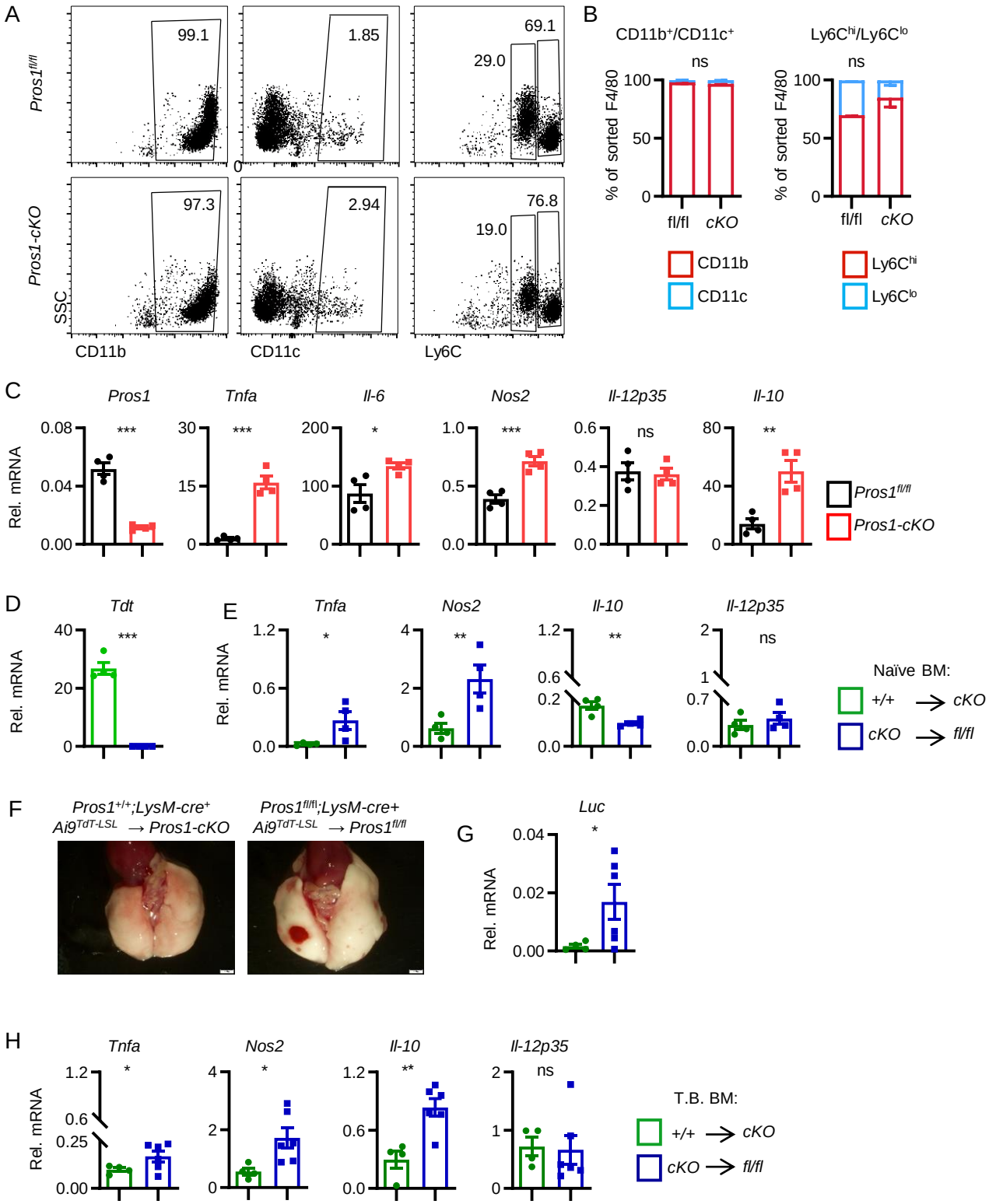
A
Pros1fl/fl
Pros1-cKO
99.1
1.85
69.1
29.0
97.3
2.94
76.8
19.0
SSC
CD11b
CD11c
Ly6C
B
CD11b+/CD11c+
Ly6Chi/Ly6Clo
ns
% of sorted F4/80
fl/fl
cKO
CD11b
CD11c
Ly6Chi
Ly6Clo
C
Pros1
Tnfa
Il-6
Nos2
Il-12p35
Il-10
Rel. mRNA
Pros1fl/fl
Pros1-cKO
D
Tdt
E
Naïve BM:
+/+ → cKO
cKO → fl/fl
F
Pros1+/+;LysM-cre+ Ai9TdT-LSL → Pros1-cKO
Pros1fl/fl;LysM-cre+ Ai9TdT-LSL → Pros1fl/fl
G
Luc
H
T.B. BM:

Fig.3: *Pros1*-deficient F4/80^{+} bone marrow-derived cells infiltrate metastatic lungs and impose inflammation in-vivo.

(A-C) Analysis of lung-infiltrating immune cells in tumor-bearing mice. F4/80^{+} cells sorted from metastatic lungs were characterized immunologically (A, B) and by mRNA expression (C). (B) Distribution of CD11b^{+}/CD11c^{+} and Ly6C^{hi}/Ly6C^{lo} from the indicated mice is shown as mean percent of F4/80^{+} cells ± SEM from 7-8 mice/group. (C) Inflammatory cytokine analysis by RT-qPCR of F4/80+ cells isolated from metastatic lungs. Each dot represents a pool of 7-8 mice/group; 3 independent experiments. Mean relative values ± SEM; P<0.0001 for *Pros1* and *Tnfα*, P=0.014, 0.0005 and 0.002 for *Il-6*, *Nos2* and *Il-10* respectively, t-test. (D-H) Adoptive transfer of *Pros1*-deficient bone marrow induces lung inflammation and supports lung-metastasis. (D-E) TdT and cytokine expression in lungs 7 weeks after BM transplantation from *Pros1*$^{+/+}$;TdT^{+} into TdT-deficient cKO (green bars) and TdT^{+};cKO into TdT-deficient *fl/fl* (blue bars) in a tumor-naïve setting. Mean ± SEM; 4 mice/group, P<0.0001, 0.018, 0.008 and 0.003 for *Tdt, Tnfα*, *Nos2* and *Il-10*, respectively; t-test. (F-H) LLC-luc cells were subcutaneously injected 4 weeks after BM transplantation. Three weeks later, lungs were isolated (F) and analyzed by RT-qPCR (G-H). Mean ± SEM; n=4-6 mice/group. P≤0.05 for *Luc, Tnfα, Nos2, and* 0.0 02for *Il-10*; t-test. ns = non-significant.

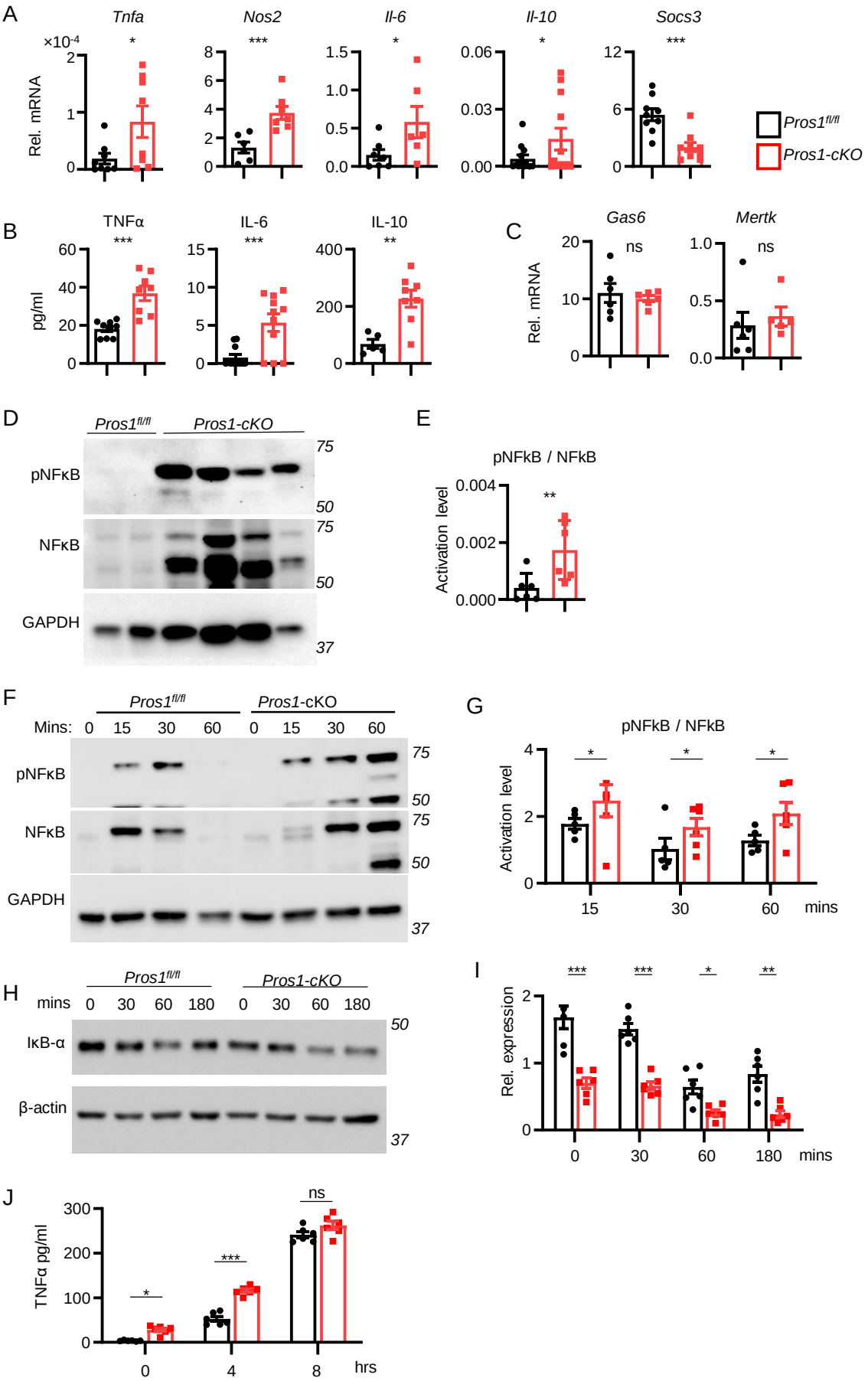
A
Tnfa
Nos2
Il-6
Il-10
Socs3
Rel. mRNA
×10-4
Pros1fl/fl
Pros1-cKO
B
TNFα
IL-6
IL-10
pg/ml
C
Gas6
Mertk
ns
Rel. mRNA
D
Pros1fl/fl
Pros1-cKO
pNFκB
NFκB
GAPDH
E
pNFkB / NFkB
Activation level
F
Mins: 0 15 30 60 0 15 30 60
pNFκB
NFκB
GAPDH
G
pNFkB / NFkB
Activation level
15 30 60 mins
H
mins 0 30 60 180 0 30 60 180
IκB-α
β-actin
I
Rel. expression
0 30 60 180 mins
J
TNFα pg/ml
ns
0 4 8 hrs

Fig. 4: *Pros1*-deficient macrophages exhibit a pro-inflammatory profile, regulated by the NFκB pathway.

Cytokine transcript levels from cultured BMDMs derived from tumor-naïve control and *Pros1*-cKO mice, measured by RT-qPCR. Relative mean expression ± SEM n=6-12 mice/group; P = 0.02, 0.001, 0.03, 0.049 and 0.0003 for *Tnfα*, *Nos2*, *Il-6, Il-10* and *Socs3,* respectively; t-test. (B) ELISA measurements of TNFα, IL-6 and IL-10 from BMDM-CM isolated from tumor-naïve *Pros1*-cKO and control mice. Average cytokine values ± SEM are shown for 8-11 mice. P=0.0001, 0.0006 and 0.001 for TNFα, IL-6, IL-10 respectively; t-test. (C) *Gas6* and *MerTK* expression in control and *Pros1*-ablated BMDMs; n = 5-6 mice/group; t-test. (D, E) Representative western blot analysis of pNFκB and NFκB from BMDMs at steady state (grown in 10% FBS), and band intensities (E, n=6/group; P=0.009). (F-I) Western blot analysis of the NFκB pathway. (F) Representative blots of cell lysates showing pNFκB, tNFκB and band intensities (G; P=0.01, 0.04 and 0.01 for 15, 30 and 60 mins, respectively) of LPS-stimulated (100 ng/ml) serum-starved BMDMs derived from tumor-naïve control and *Pros1*-cKO mice, and of IκB-α (H, I; ***P<0.0001, *P=0.05 and **P=0.001). β-actin served as loading control. Graphs indicate the mean ± SEM; n=6; 2-way ANOVA. (J) ELISA measurements of TNFα production by control and *Pros1*-cKO serum-starved and LPS-treated (500ng/ml) BMDMs at 0, 4 and 8 hrs post LPS challenge. Average ± SEM; n=6-8 mice (*P=0.048, *** P<0.0001,); 2-way ANOVA. ns = non-significant.

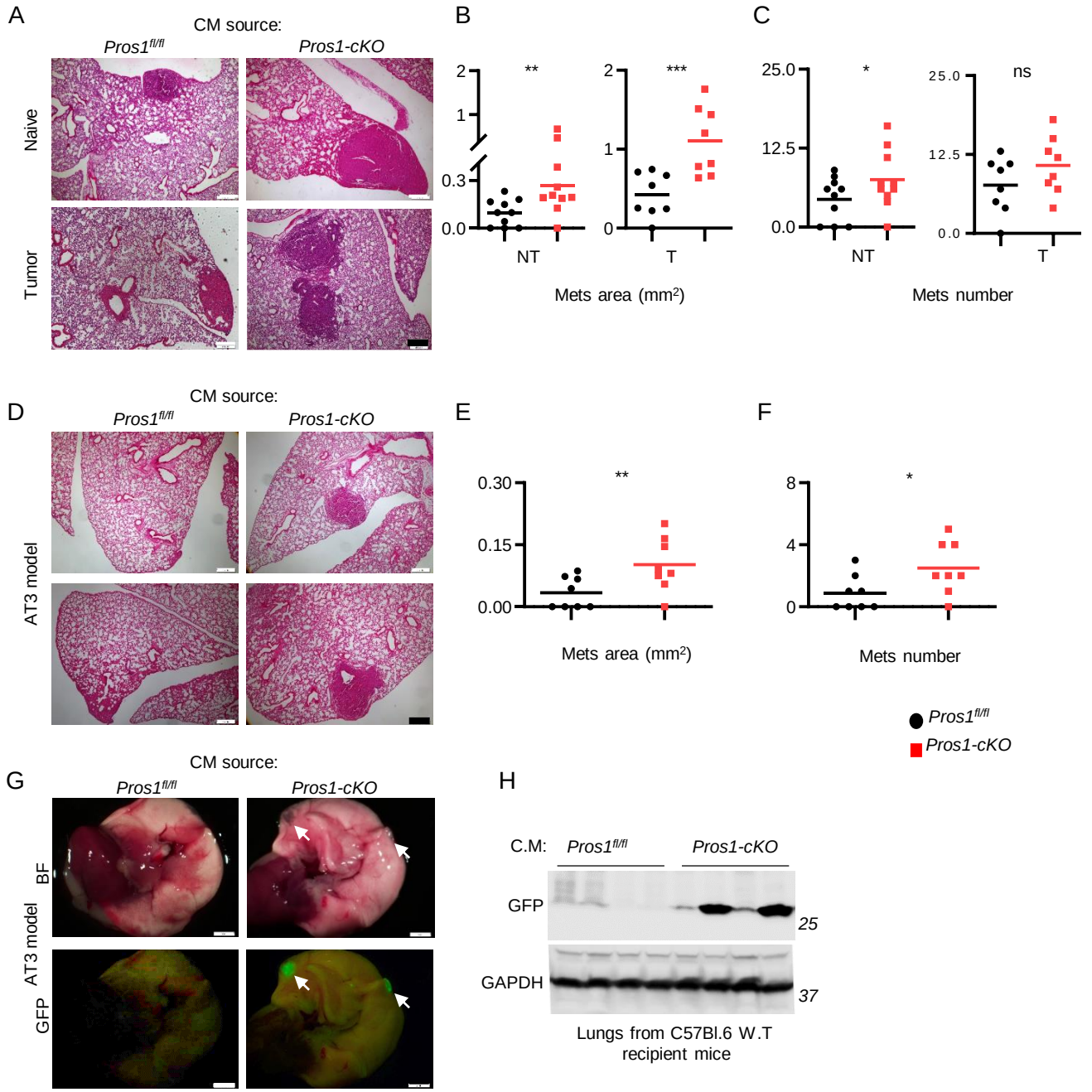
A
CM source:
Pros1fl/fl
Pros1-cKO
Naive
Tumor
B
**
***
2
1
0.3
0.0
NT
T
Mets area (mm2)
C
*
ns
25.0
12.5
0.0
NT
T
Mets number
D
CM source:
Pros1fl/fl
Pros1-cKO
AT3 model
E
**
0.30
0.15
0.00
Mets area (mm2)
F
*
8
4
0
Mets number
Pros1fl/fl
Pros1-cKO
G
CM source:
Pros1fl/fl
Pros1-cKO
BF
AT3 model
GFP
H
C.M:
Pros1fl/fl
Pros1-cKO
GFP
25
GAPDH
37
Lungs from C57Bl.6 W.T
recipient mice

Fig.5: Enhanced metastatic potency of *Pros1*-deficient BMDMs.

(**A-C**) LLC cells were educated for 24 hrs with conditioned medium (CM) from BMDMs isolated from non-tumor (NT) or tumor bearing (T) control (*Pros1*$^{fl/fl}$) and *Pros1*-cKO mice. Educated cells were injected into wild type mice. Lung metastasis were evaluated at 3 weeks by H&E. Representative H&E-stained lung sections (A), average area (B, P=0.01 (NT), 0.001 (T)) and number of metastases (C, P=0.05 (NT), ns=non-significant (T)) are plotted. N=8-10 mice/group; t-test. (D-F) GFP-labelled AT3 cells were educated for 96 hrs with the indicated BMDM-CM and injected into host wild-type mice. Lung metastases were evaluated 3 weeks later. N=8 mice/group. Representative H&E lung sections (D); average metastatic area (E), and number (F) are shown. The horizontal line represents the mean value. P=0.01, and 0.02 for E, F, respectively; t-test. Scale=200 µm. (G-H) Representative images of freshly-isolated lungs described in (D) as observed under bright field (BF) and fluorescent illumination (GFP). Arrows indicate metastatic foci. Scale=2 mm. (H) Representative western blot for GFP content in lungs shown in G. GAPDH was used as a loading control. N=4/group.

Maimon et al – Figure 6

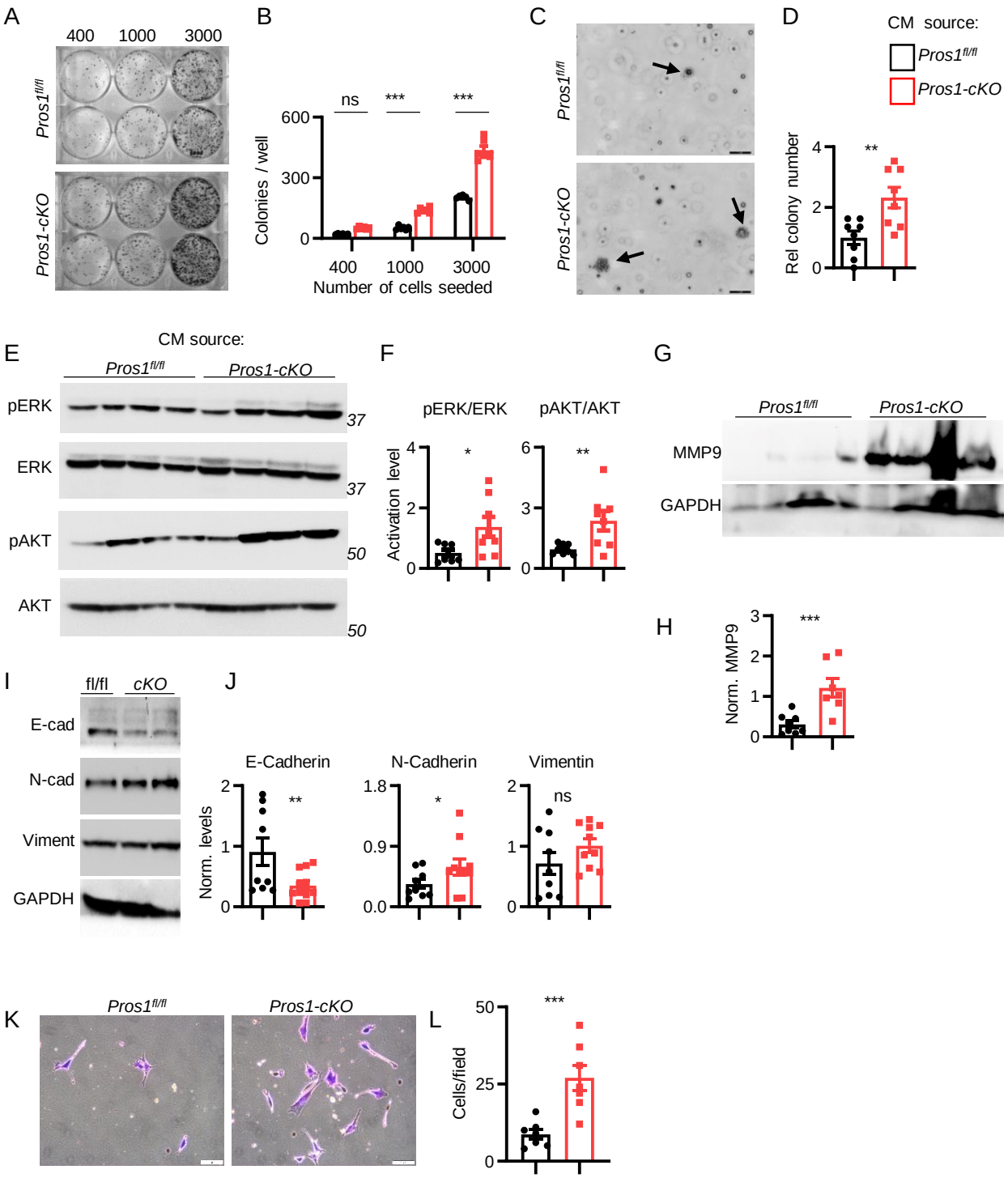

Fig. 6: Conditioned medium from *Pros1*-ablated BMDMs enhances LLC cancer cell aggressiveness.

LLC cells were educated (24 hrs) by the indicated conditioned medium and subject to a battery of in vitro assays. (A, B) Colony survival after 10 days. (A) Representative images (# cells plated/well is indicated) and (B) quantification of surviving colonies. The mean ± SEM; n= 6 mice/group; ***P<0.0001; 2-way ANOVA. (C) Representative images and (D) quantification of soft agar colonies (arrows) after 21 days. Bar=50µm. Average ± SEM; n=8 mice/group, P=0.002; t-test. (E) Representative western blots and (F) quantifications showing ERK and AKT activation from educated LLC cells. N=8 mice/group; 3 independent experiments. The average ratio ± SEM is plotted. P=0.018, 0.006 for pERK and pAKT, respectively (t-test). Representative western blot (G) and quantifications (H) for MMP9 protein in lungs of metastatic mice. N=7-8 mice/group in 2 independent experiments. The average ratio ± SEM is plotted, P=0.001, t-test. A representative western blot (I) and quantifications (J) showing E-cadherin, N-cadherin and Vimentin in educated LLC cells. N=9-10 mice/group in 3 independent experiments. The average ratio ± SEM is plotted, P=0.009, 0.04 for E-cadherin and N-cadherin respectively, t-test. (K, L) Invasion assay: representative images (K) and quantifications (L) of cells that invaded through Matrigel, following education with the indicated CM; scale=50µm. (L) The average cell number ± SEM of invaded cells from 7-10 different fields, n=7 mice/group in three independent experiments. P=0.0007, t-test. ns = non-significant.

Maimon et al – Figure 7

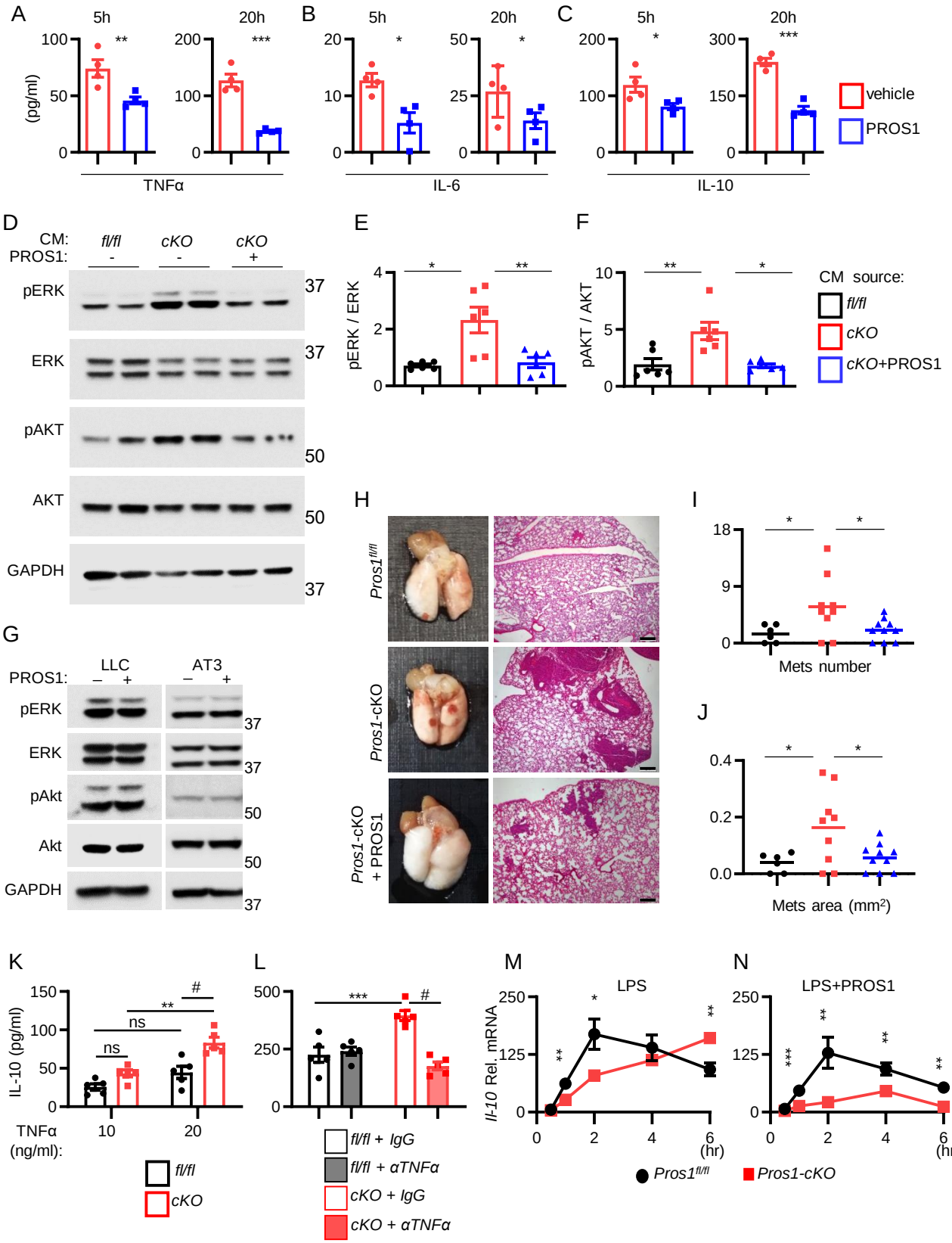

Fig. 7: Exogenous PROS1 dampens the inflammatory signature of *Pros1*-cKO BMDMs and mitigates metastasis in-vivo.

(A-C) Cytokine secretion by LPS-stimulated (100 ng/ml) tumor-naïve *Pros1*-cKO BMDMs, incubated with vehicle or PROS1 (25nM). ELISA measurements at 5, 20 hrs. Mean ± SEM; n=4/group. TNFα (A, **P=0.007; ***P=0.0001), IL-6 (B, *P=0.03 and 0.05), IL-10 (C, *P=0.02; ***P<0.0001); t-test**.** (D-F) PROS1 reverses the pro-metastatic potential of cKO-BMDMs. Representative western blot (D), quantification of ERK (E; *P=0.03; **P=0.01) and AKT (F; **P=0.003; *P=0.02) activation in LLC cells educated with CM from $BMDM^{fl/fl}$ or cKO cells, with or without PROS1 (25 nM). Two mice of 6 are shown/group; 1-way ANOVA. (G) Western blot analysis shows no direct activation of AKT or ERK by PROS1-treated LLC cells (25nM, 24 hrs). A representative blot of three experiments is shown. (H-J) PROS1 suppresses the metastasis-inducing potential of cKO-BMDMs in-vivo. (H) wild type mice (n=6-10/group) were inoculated with educated cells as described in D. Lungs were assessed for metastases 3 weeks later (left). H&E sections (right) were used to quantify the average metastatic area (I; P=0.03) and number (J; P=0.04); 1-way ANOVA. The horizontal line marks the mean tumor weight. Scale=200 µm. (K-L) TNFα regulates IL-10 secretion in cKO BMDMs. (K) ELISA measurements of IL-10 secretion by TNFα-stimulated (10 and 20 ng/ml; 24 hrs) control and cKO BMDMs. Mean ± SEM; n=5 mice/group. **P=0.0014; #P=0.002, ns=non-significant. 2-way ANOVA. (L) ELISA measurements of IL-10 secretion from LPS-stimulated (100ng/ml; 24 hrs) $BMDM^{fl/fl}$ or cKO, pre-treated with IgG or anti-TNFα neutralizing antibody. The mean ± SEM; n=5; ***P=0.0006; #P<0.0001; 2-way ANOVA; (M-N) Relative *Il-10* mRNA levels of LPS-simulated (100 ng/ml) BMDMs without (M; P=0.002, 0.02, 0.004 at 1,2,6 hrs) or with PROS1 (25 nM) (N; P<0.0001, P=0.01 and 0.004 at 1,2,6 hrs). Relative mean ± SEM; n=5 mice/group; holm-sidak multiple t-test.

Maimon et al – Figure 8

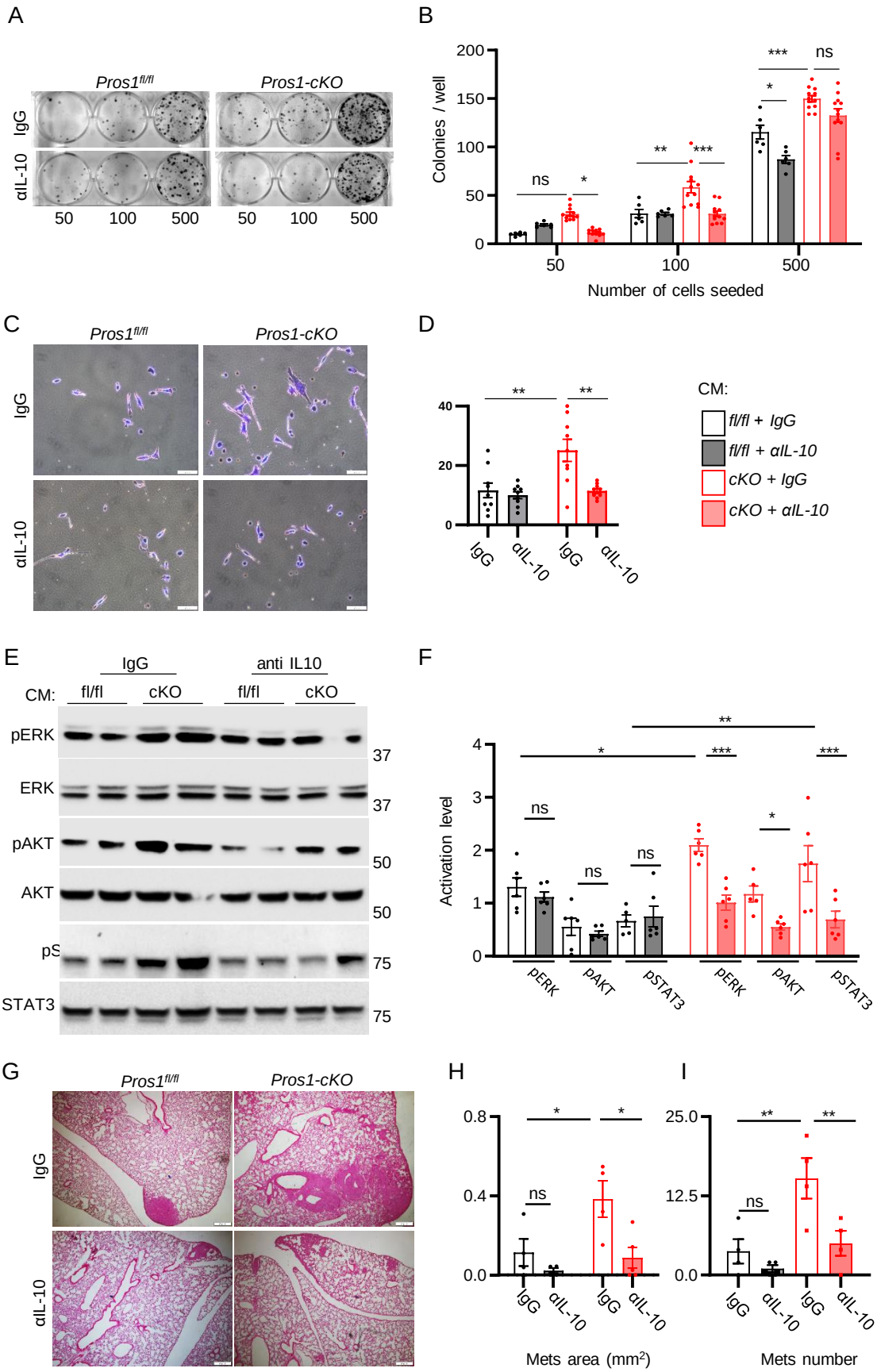

Fig.8: Neutralization of IL-10 in *Pros1*-cKO CM reduced LLC aggressiveness and suppressed in vivo metastasis.

LLC cells were educated by the indicated CM with control (IgG) or anti IL-10 neutralizing antibodies (αIL-10) for 24 hrs and subject to a battery of in vitro assays. (A, B) Colony survival after 10 days. Representative images of educated cells (plated at different densities, as indicated, A) and quantification of colonies (B). The mean ± SEM; n=6-12 mice/group; 3 independent experiments. *P=0.02; **P=0.004; ***P<0.0001; 2-way ANOVA. (C-D) Matrigel invasion assay. Representative images (C) and quantification (D) of educated cells that traversed the ECM-coated membrane without or with IL-10 neutralization. Scale=50μm. (D) The average cell number from 7-9 different fields ± SEM, 4-5 mice/group, two independent experiments. P=0.0017 and 0.0014; 2-way ANOVA. (E) Representative western blots and quantifications (F) of ERK, AKT and STAT3 activation from educated LLC cell lysates. Band intensities were calculated from 5-6 mice/group, 2 independent experiments. The average ratio (phosphorylated/total) ± SEM is plotted. P values for control vs cKO with IgG: P=0.04 (ERK) and 0.002 (STAT3) and for cKO with IgG vs cKO with αIL-10 are 0.001 (ERK), 0.05 (AKT), 0.001 (STAT3); 2-way ANOVA. (G-I) Educated LLC cells described above were subcutaneously injected into the flank of WT mice and three weeks later lung metastasis was evaluated. (G) Representative images of H&E sections from lungs, Scale=200μm. (H-I) Scoring of lung metastases, the average metastatic area (H) and number (I) ± are shown. P=0.04 and 0.02 for H, and P=0.01 and 0.008 for I; 2-way ANOVA. ns = non-significant.

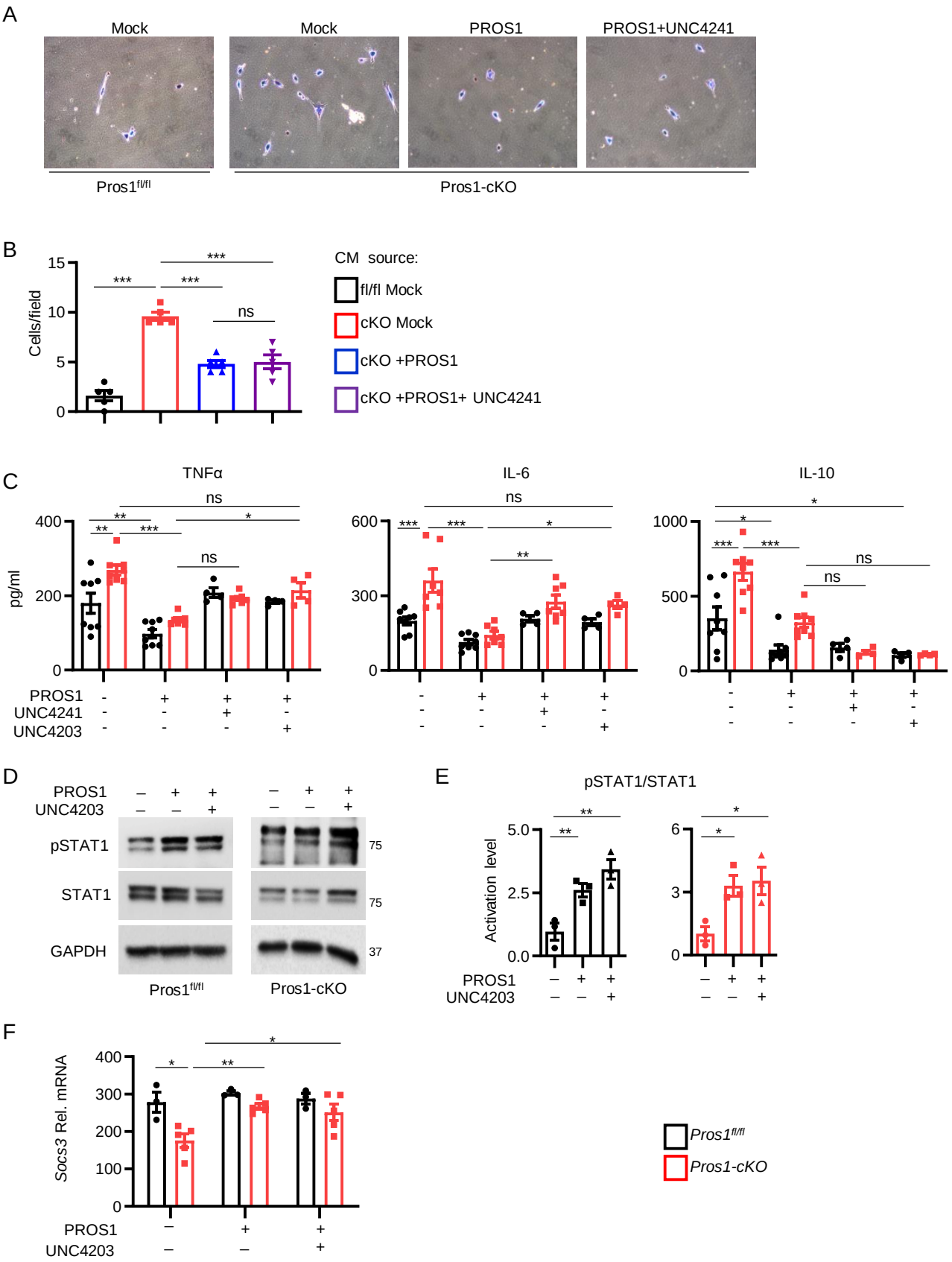
A
Mock
Mock
PROS1
PROS1+UNC4241
Pros1fl/fl
Pros1-cKO
B
Cells/field
CM source:
fl/fl Mock
cKO Mock
cKO +PROS1
cKO +PROS1+ UNC4241
C
TNFα
IL-6
IL-10
pg/ml
PROS1
UNC4241
UNC4203
D
PROS1
UNC4203
pSTAT1
STAT1
GAPDH
Pros1fl/fl
Pros1-cKO
E
pSTAT1/STAT1
Activation level
PROS1
UNC4203
F
Socs3 Rel. mRNA
PROS1
UNC4203
Pros1fl/fl
Pros1-cKO

Fig. 9: Distinct requirements for the MERTK kinase activity in PROS1-mediated regulation of TNFα and IL-6 versus IL-10.

(A-B) Matrigel invasion assay. LLC cells were educated with BMDM-CM from fl/fl or cKO BMDMs (mock), or supplemented with PROS1 or with PROS1 + UNC4241 (pan-TAM kinase inhibitor). Representative images (A, scale=50μm) and quantifications (B) of cells that invaded through Matrigel. Graphs present the average cell numbers from 7-10 different fields ± SEM, 4-5 mice/group, 2 independent experiments. P≤0.0001, 1-way ANOVA. (**C**) ELISA measurements of secreted cytokines in CM of control and cKO BMDMs. Serum-starved BMDMs were treated with PROS1 (25 nM) alone or with 500 nM UNC4241 (pan-TAM) or UNC4203 (MER-specific) inhibitors for 1 hour, then stimulated with LPS for 24 hrs. Average values ± SEM are shown for 4-8 mice, 2 independent experiments. TNFα: ***P = 0.001, **P≤0.005, *P = 0.05; IL-6: *** P≤0.0004, **P=0.005, *P≤0.05; IL-10: ***P≤0.0004, * P≤0.05; 2-way ANOVA. (D-F) MERTK kinase activity is not essential for STAT1 activation by PROS1. Representative western blots (D) and quantification (E) of STAT1 activation in LPS-stimulated BMDMs either without or with PROS1 and UNC4203 (500 nM), as indicated. GAPDH served as a loading control. Graphs present the average values ± SEM, 6 mice/group; 2 independent experiments. Each dot represents a pool of 2 mice/group. **P≤0.01 and *P≤0.012 for *fl/fl* and cKO, respectively; 1-way ANOVA. (F) *Socs3* relative mRNA levels from BMDMs described in D. Mean ± SEM; n=6-10 mice; each dot represents a pool of 2 mice. *P≤0.05; 2-way ANOVA.

Maimon et al – Figure 10

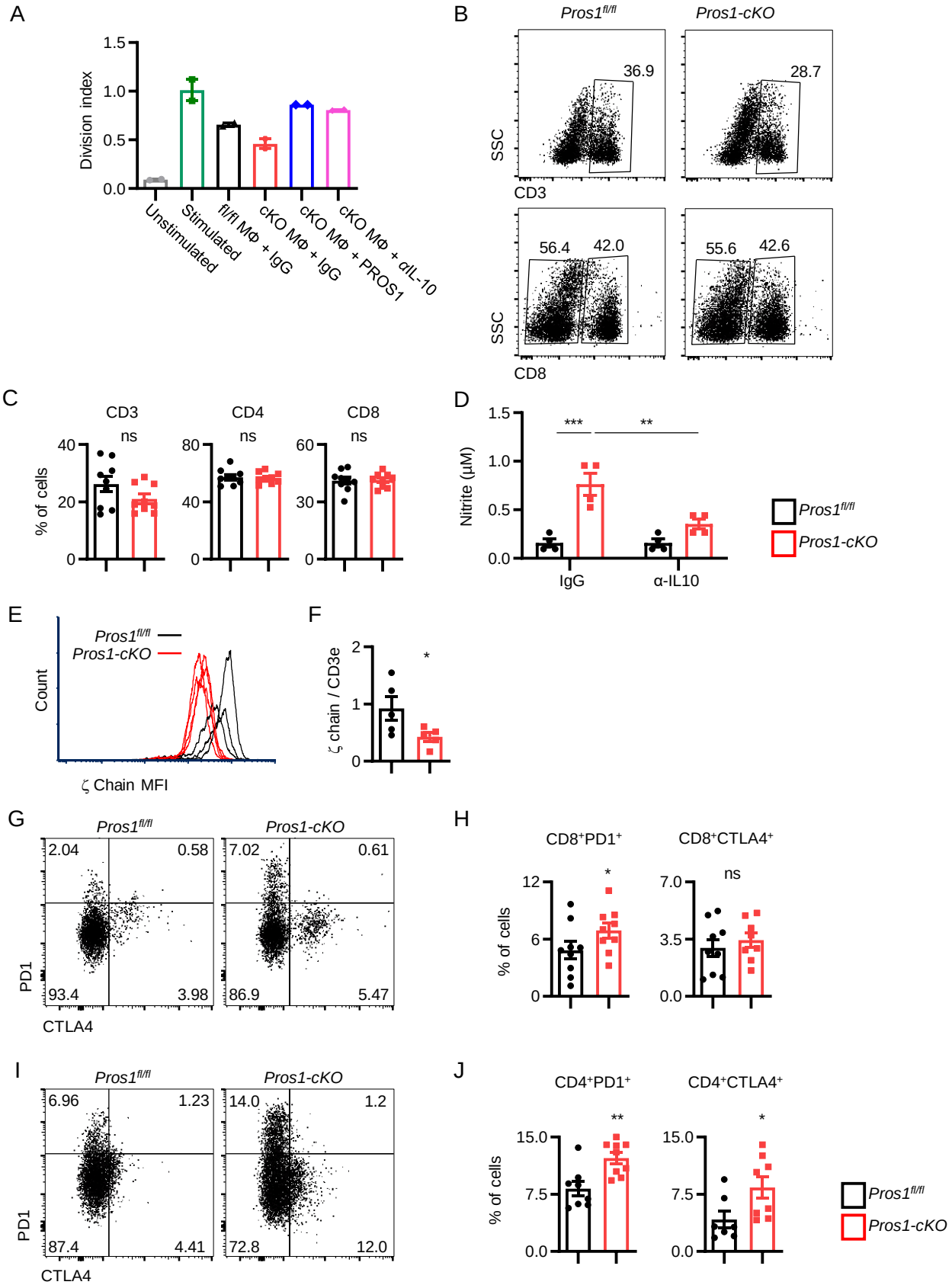

Fig. 10: PROS1 inhibition in myeloid cells modulates the T cell response.

(A) Ex-vivo T cell proliferation assay. Total $CD3^+$ T cells were left unstimulated (grey bar) or stimulated with anti-CD3/CD28 antibodies and labelled with CellTrace. Stimulated T cells were left alone (green bar) or co-cultured with control IgG and $F4/80^+$ macrophages (MΦ) sorted from metastatic lungs of fl/fl (black bar) or cKO (red bar) mice, purified PROS1 (50 nM, blue bar), or IL-10 neutralizing IgG (αIL-10; 5µg/ml, pink bar) for 72 hrs. Bars represent the average division index ± SEM from two independent experiments. Each dot represents a pool of 7-9 mice. (B) Representative FACS plots and quantifications (C) of $CD3^+$ or $CD8^+$ populations in $CD45^+$-gated cells from metastatic lungs of the indicated genotype. Mean percent ± SEM; n=9 mice/group; 3 independent experiments; t-test. (D-J) Impaired activation of metastasis-associated T cells in Pros1-cKO mice. (D) Nitrite levels measured in T cell-macrophages co-culture medium, with control IgG or αIL-10 neutralizing antibody. ***P=0.0002; **P=0.005; 2-way ANOVA. (E-J) Analysis of T cells receptor (TCR) ζ chain and the immune checkpoint molecules PD-1 and CTLA-4 in T cells from metastatic lungs. (E) Representative FACS histograms show the mean fluorescent intensity (MFI) for ζ chain from the indicated metastatic lungs analyzed for CD3ε and TCR-ζ chain. (F) Relative MFI of ζ chain/CD3ε from 5 mice/group ± SEM, in 2 independent experiments; P=0.026, t-test. (G-J) Representative FACS plots for $CD45^+CD3^+$-gated cells from the indicated metastatic lungs stained for PD-1 and CTLA-4 on $CD8^+$ (G) and $CD4^+$ (I) cell populations, and their quantifications (H, J, respectively). The mean percent ± SEM; n=8-9 mice/group; 2 independent experiments. G; P=0.05 I; P=0.0017 for PD1 and 0.019 for CTLA-4, t-test. ns=non-significant.

Maimon et al – Figure 11

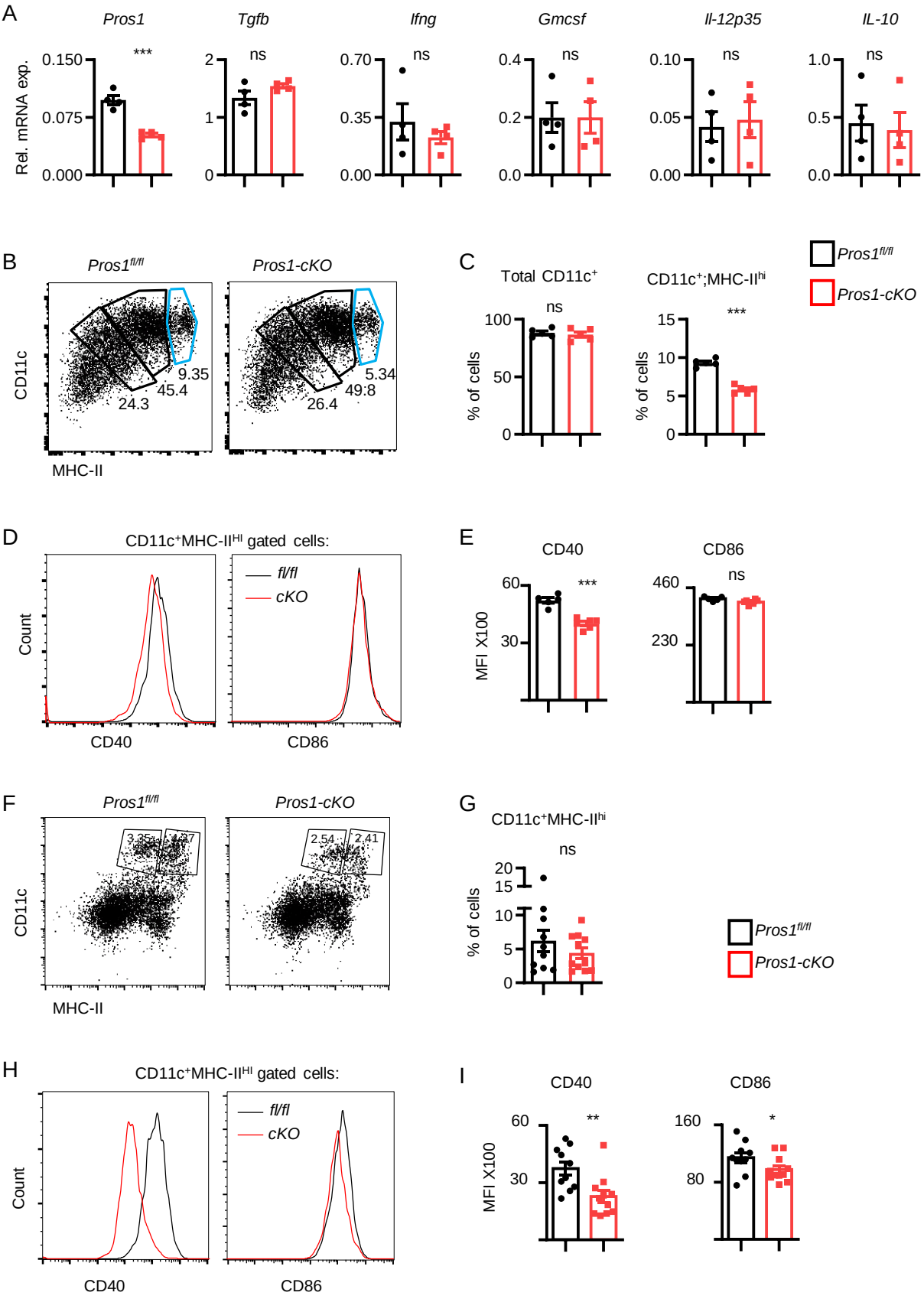

Fig.11: Impaired maturation and incomplete expression of co-stimulatory molecules by dendritic cells following partial deletion of *Pros1*.

(A-E) Analysis of BM-DCs. (A) Relative mRNA expression of the indicated cytokines in GM-CSF induced BMDCs from *Pros1*$^{fl/fl}$ control and *Pros1*-cKO mice, measured by RT-qPCR. Mean ± SEM; n=4 mice/group; 2 independent experiments. *** P=0.0002, t-test. (B, C) Representative FACS plots of CD45^{+} gated cells analyzed for CD11c^{+} cells expressing different MHC-II intensities. The light blue gate indicates the MHC-II^{hi} cells (B) and quantification (C) of CD45^{+} gated cells analyzed for total CD11c and CD11c^{+}MHC-II^{hi} (light blue gate). Mean percent ± SEM; n=4 mice/group, ***P<0.0001 and non-significant, t-test. (D) Representative histograms and quantification (E) of CD11c^{+}MHC-II^{hi} gated cells (light blue gate) further analyzed for CD40 and CD86 expression. MFI ± SEM; n=5-6 mice/group, ***P=0.0001, t-test. (F-I) Analysis of DCs from metastatic lungs. (F) Representative FACS plots and (G) quantification of CD45^{+} gated cells from fl/fl and cKO metastatic lungs analyzed for total CD11c^{+}MHC-II^{hi} cells. Mean percent ± SEM; n=10-11 mice/group; 2 independent experiments; t-test. (H) Representative histograms and (I) quantification of CD11c^{+}MHC-II^{hi} gated cells analyzed for CD40 and CD86 expression. Graphs present the MFI ± SEM; n=10-11 mice/group, P=0.003 and 0.03 for CD40 and CD86 respectively, t-test. ns = non-significant.